Isobar-model partial-wave analysis of $\pi N \to \pi\pi N$ in the c.m. energy range 1320–1930 MeV

D. Mark Manley, Richard A. Arndt, and Yogesh Goradia*

Department of Physics, Virginia Polytechnic Institute and State University, Blacksburg, Virginia 24061

Vigdor L. Teplitz

Arms Control and Disarmament Agency, Strategic Affairs Division, Washington, D.C. 20451
and Department of Physics, University of Maryland, College Park, Maryland 20742
(Received 16 March 1984)

We study the reactions $\pi N \to \pi\pi N$ in the center-of-mass energy range 1320–1930 MeV within the framework of the isobar model. The present analysis includes over 30% more events than the most extensive previous analysis. Data for $\pi^- p \to \pi^+\pi^- n$, $\pi^- p \to \pi^0\pi^- p$, $\pi^+ p \to \pi^0\pi^+ p$, and $\pi^+ p \to \pi^+\pi^+ n$ are simultaneously fitted assuming production of ϵ, ρ, $\Delta(P_{33})$ and $N^*(P_{11})$. The cross section for $\pi^- p \to \pi^0\pi^0 n$ is predicted and found to be in good agreement with experiment. $\pi N \to \pi N^*$ amplitudes for $I = \frac{1}{2}$ are investigated for the first time. We confirm the existence of a significant πN^* decay for the second P_{33} resonance and determine that πN^* is the dominant inelastic channel for the P_{31} partial wave. The ρN decay of the G_{17} wave is observed for the first time. Evidence is found for unestablished resonances near 1900 MeV in the S_{11}, P_{11}, P_{13}, and F_{15} partial waves. We also discuss evidence for a second F_{35} resonance. Signs of resonant amplitudes determined from this analysis are compared with results of previous analyses and with predictions from several models.

I. INTRODUCTION

Dalitz plots reveal that nonstrange baryon resonances decay predominantly into quasi-two-body channels. Such decays are typically well described by isobar models. By studying the inelastic reactions $\pi N \to \pi\pi N$, one hopes to detect πN resonances and to extract couplings of the resonances to such quasi-two-body channels as ϵN, ρN, $\pi\Delta$, and πN^*. Early analyses of these reactions have been few in number, due mainly to lack of data, complexity of the analysis, and expense in both time and money. The consistency of early results for $\pi N \to \pi\Delta$ amplitudes between independent Berkeley-SLAC[1] and Saclay[2] groups was encouraging. Unfortunately, the results for $\pi N \to \rho N$ amplitudes were in poorer agreement. Resonance couplings to the $\pi N^*(P_{11})$ channel have been previously investigated only for $I = \frac{3}{2}$ by the Imperial College group.[3]

Several theoretical models[4–8] have been suggested to explain the results of previous partial-wave analyses. Because of the above inconsistencies between the earlier Berkeley-SLAC and Saclay analyses, such models have necessarily been able to compare only a small set of amplitudes common to both studies. For this reason, in part, we performed an independent partial-wave analysis. For the first time, both $\pi^- p$ and $\pi^+ p$ interactions are investigated simultaneously with $\pi N \to \pi N^*(P_{11})$ amplitudes included in the search. We have also investigated the importance of some of the higher partial waves by searching g-wave amplitudes.

In Sec. II, we discuss the data used in our analysis. In Sec. III, we summarize the formulas used for our isobar model and present explicit descriptions of some of our parametrizations. In Sec. IV, we discuss the details of our fitting algorithm. In Sec. V, we discuss our analysis procedure. In Sec. VI, we present and discuss the results of our analysis. In Sec. VII, we compare our results with those of previous analyses. We also compare signs of the experimental resonance couplings to predictions of several theoretical models. Finally, in Sec. VIII, we summarize the main findings of our work.

II. THE DATA

For the present analysis, we have gathered data from several large bubble-chamber experiments[9–11] spanning the center-of-mass (c.m.) energy range 1320–1930 MeV. A total of 241214 events were included in our analysis. We had access to all data previously analyzed in this energy range by the Berkeley-SLAC collaboration[1] except for 6372 $\pi^0\pi^+ p$ events between 1830 and 1870 MeV and all $\pi^+\pi^+ n$ events from a Berkeley-Riverside experiment.[9] We also had several thousand additional events from more recent experiments.[10] The total sample of events was divided into 22 nonoverlapping energy bins which were analyzed separately; i.e., our analysis was an energy-independent one. Table I summarizes the number of events fitted at each energy. We attempted to bin events in energy intervals of 20 MeV whenever more than 10000 events were available at a given energy. However, due to insufficient data, it was necessary to increase the bin width to either 30 or 40 MeV below 1390 MeV, above 1710 MeV, and between 1550 and 1610 MeV, the "energy gap" in the Berkeley-SLAC analysis.

Each subsample of data was fitted using as c.m. energy the central value for each bin. As discussed in Ref. 12, the events within each bin were modified to satisfy the relationship

TABLE I. Summary of the number of events analyzed at each energy.

W (MeV)	$\pi^+\pi^- n$	$\pi^0\pi^- p$	$\pi^0\pi^+ p$	$\pi^+\pi^+ n$	Total
1340±20	1664	11	0	0	1675
1375±15	3893	145	15	2	4055
1400±10	3646	826	63	15	4550
1440±10	3790	1339	207	48	5384
1460±10	2074	971	152	36	3233
1480±10	7246	3776	537	128	11 687
1500±10	6224	4055	1160	250	11 689
1520±10	5650	4671	795	143	11 259
1540±10	6230	5320	1115	183	12 848
1565±15	2237	1598	2704	481	7020
1595±15	3065	1962	2864	483	8374
1620±10	0	0	4203	621	4824
1640±10	7437	4177	7939	1013	20 566
1660±10	7411	4273	4071	752	16 507
1680±10	8784	5340	4999	847	19 970
1700±10	8377	5394	5375	1007	20 153
1725±15	6265	4594	5679	524	17 062
1755±15	5442	4200	1316	18	10 976
1790±20	1966	1352	4715	228	8261
1830±20	3543	2223	2322	0	8088
1870±20	4342	3382	8190	557	16 471
1910±20	6036	4081	6445	0	16 562
Total	105 322	63 690	64 866	7336	241 214

$$W^2 + m_N^2 + 2m_\pi^2 = \sum_i W_i^2 \, ,$$

where W is the central energy of the bin, $m_N = 939$ MeV is the mass of the nucleon, $m_\pi = 139$ MeV is the mass of the pion, and W_i is the subenergy of the ith pair of final-state particles $(i=1,2,3)$. For each event, our procedure required calculating

$$W_i^2 = W_i^2(\text{threshold}) + \Delta W_i^2$$

and scaling the three ΔW_i^2 by the same factor.

III. THE ISOBAR MODEL

In this section, we summarize the main ingredients of our isobar model. Detailed discussions of the formalism have been presented elsewhere.[13]

The reactions $\pi N \rightarrow \pi\pi N$ are assumed to proceed through four intermediate quasi-two-body channels:

$$\pi N \rightarrow \pi\Delta(P_{33}) \, ,$$

$$\pi N \rightarrow \rho N \, ,$$

$$\pi N \rightarrow \epsilon N \, ,$$

$$\pi N \rightarrow \pi N^*(P_{11}) \, .$$

Here, ϵ represents the strong, s-wave $\pi\pi$ isoscalar interaction. The importance of the ϵN, ρN, and $\pi\Delta$ channels is now well established. However, the ρN and $\pi\Delta$ channels alone are known to be insufficient for simultaneously describing the reactions $\pi^+ p \rightarrow \pi^0\pi^+ p$ and $\pi^+ p \rightarrow \pi^+\pi^+ n$ above about 1600 MeV.[3] Because πN mass spectra reveal

that N^* isobars are present in this energy range, our analysis includes the least massive N^*, the $P_{11}(1440)$ or Roper resonance. Other N^* isobars were investigated and found to be relatively unimportant (see Sec. V).

The total amplitude for a given charge channel can be written as a coherent sum over all isobars and partial waves:

$$\langle f \mid T \mid i \rangle = \sum A_{n_1} X_{n_1} + \sum A_{n_2} X_{n_2} + \sum A_{n_3} X_{n_3} \, . \tag{3.1}$$

Here, the index n_γ denotes the collection of quantum numbers that describe the nth partial wave associated with representation γ, which describes, for $\pi N \rightarrow \pi\pi N$, the case in which particle γ is the spectator and particles α and β form the isobar $[(\alpha,\beta,\gamma)=(1,2,3)$ and cyclic permutations]. We define particles 1 and 2 to be the final-state pions and particle 3 to be the final-state nucleon. The X_{n_γ} are complex basis functions that depend on four kinematic variables for describing an event at fixed total c.m. energy W. The A_{n_γ} are partial-wave amplitudes which are treated as variable, complex parameters.

As usual, we approximated the A_{n_γ} as constants for fixed total c.m. energy with all known functional dependence on energy and angular variables absorbed by the X_{n_γ}. This approximation is believed to be inconsistent with two-body unitarity which requires that the A_{n_γ} depend on the isobar subenergy as well as on W. In an early work, Aaron and Amado suggested that unitarity might impose a rapid subenergy variation on the partial-wave amplitudes.[14] They later realized, however, that this variation was not present in the physical amplitudes since it was associated with poles on an unphysical sheet.[15] This

point was noted independently by Aitchison and Gold-ing.[16] Aitchison and Brehm have studied this problem extensively within an isobar model that incorporates unitarity and analyticity in the isobar subenergy channels.[17] Their work indicates that the variation with subenergy is smooth and not very fast. We infer from their calculations that the major subenergy variation is manifested by a nonzero range in the barrier-penetration factor, which we discuss below. This problem has been investigated experimentally by the Imperial College group.[3] They fitted $\pi N \rightarrow \pi\pi N$ events at 1610 MeV by dividing the Dalitz plot into two halves. By fitting the two halves separately, they concluded that the effects of subenergy dependence were small.

The basis functions can be expressed by

$$X_{n_\gamma} = [C_{n_\gamma} K_{n_\gamma} B_{l_f}(p_\gamma) R^{-1}] D(q_\gamma) , \qquad (3.2)$$

where the quantity in brackets describes production of the (α,β) isobar and spectator particle γ from the πN initial state. C_{n_γ} is an isospin coefficient, K_{n_γ} is a kinematic factor describing all angular dependence, $B_{l_f}(p_\gamma)$ is a barrier-penetration factor, and R is a normalization integral. The subscript l_f denotes the orbital angular momentum between the isobar and spectator, while $\vec{p}_\gamma$ is the c.m. momentum of the isobar. $D(q_\gamma)$ is a quasi-two-body amplitude that describes the propagation and decay of the isobar, where $\vec{q}_\gamma$ is the relative momentum of the (α,β) pair.

The isospin coefficients are given by

$$C_{n_1} = C(1,\tfrac{1}{2},I;i_\pi,i_N,i)C(I_2,I_3,I_r;i_2,i_3,i_r)C(I_r,I_1,I;i_r,i_1,i)a_1 , \qquad (3.3a)$$

$$C_{n_2} = C(1,\tfrac{1}{2},I;i_\pi,i_N,i)C(I_1,I_3,I_r;i_1,i_3,i_r)C(I_r,I_2,I,i_r,i_2,i)a_2 , \qquad (3.3b)$$

$$C_{n_3} = C(1,\tfrac{1}{2},I;i_\pi,i_N,i)C(I_1,I_2,I_r,i_1,i_2,i_r)C(I_r,I_3,I;i_r,i_3,i)a_3 , \qquad (3.3c)$$

where $C(j_1,j_2,J;m_1,m_2,M)$ is a Clebsch-Gordan coefficient and the a_γ are normalization coefficients. For the charge channels with like-charge final-state pions, $a_1 = a_2 = 1/\sqrt{2}$ and $a_3 = 1$. For the charge channels with unlike-charge final-state pions, $a_1 = a_2 = 1$ and $a_3 = \sqrt{2}$. In the Clebsch-Gordan coefficients above, I and i are the total isospin and its z projection, I_r and i_r are the isospin and projection of the isobar, I_γ and i_γ are the isospin and projection of final-state particle γ, and i_π and i_N are the isospin projections for the initial pion and nucleon.

The kinematic factor is given by

$$K_{n_\gamma} = C(\tfrac{1}{2},l_i,J;\mu_i,0,\mu_i)[(2l_i+1)/(4\pi)]^{1/2}[4\pi/(2l_r+1)]^{1/2}$$

$$\times \sum_m [C(\tfrac{1}{2},l_r,S;\mu_f,m,\mu_f+m)C(S,l_f,J;\mu_f+m,\mu_i-\mu_f-m,\mu_i)Y_{l_r,m}(\hat{q}_\gamma)Y_{l_f,\mu_i-\mu_f-m}(\hat{p}_\gamma)] , \qquad (3.4)$$

where

$J = $ total angular momentum,

$l_i = $ orbital angular momentum between the initial pion and target,

$l_f = $ orbital angular momentum between the isobar and spectator,

$l_r = $ orbital angular momentum of the isobar decay products,

$S = $ total spin of isobar and spectator,

$\mu_i = $ spin projection of the initial nucleon,

$\mu_f = $ spin projection of the final nucleon.

Our barrier-penetration factors are presented in Table II. We used the Blatt-Weisskopf form[18] suggested by the Berkeley-SLAC group.[1] A general argument for this form has been given by von Hippel and Quigg.[19] We assumed for all isobars an interaction radius, $R = 0.25$ fm, which was found to be a reasonable choice by the Saclay group[2] and by Longacre.[20] We checked this assumption by refitting data at 1700 and 1870 MeV with $R = 0.5$ fm and with $R = 1.0$ fm. (At lower energies, the isobar momenta are sufficiently small that effects of a nonzero range are expected to be negligible.) Solutions were generated at these energies starting from the final solutions previously obtained with $R = 0.25$ fm. When R was increased to 0.5 fm, χ^2 decreased by 3 at 1700 MeV and by

TABLE II. Blatt-Weisskopf barrier-penetration factors $B_{l_f}(p_\gamma)$. $x = p_\gamma R$, where $R = 0.25$ fm is the interaction radius.

l_f	$B_{l_f}(p_\gamma)$
0	1
1	$x/(1+x^2)^{1/2}$
2	$x^2/(9+3x^2+x^4)^{1/2}$
3	$x^3/(225+45x^2+6x^4+x^6)^{1/2}$
4	$x^4/(11\,025+1575x^2+135x^4+10x^6+x^8)^{1/2}$

34 at 1870 MeV. However, when R was increased to 1 fm, χ^2 increased by about 200 at both energies. Thus, we conclude that the data require a small interaction radius in our energy range. From a quadratic fit of χ^2 versus R at 1700 and 1870 MeV, we estimate the optimum value of R to be about 0.4 fm. Our choice of 0.25 fm is justified, however, by the small change in our solutions when R was increased to 0.5 fm.

Our decay amplitudes are described through use of the Watson final-state interaction theorem,[21]

$$D(q_\gamma) = (W_\gamma/q_\gamma^{2l_r+1})T_{l_r} .$$ (3.5)

Here, W_γ is the subenergy of the (α,β) pair and

$$T_{l_r} = e^{i\delta l_r}\sin\delta l_r ,$$

where δl_r is the complex elastic phase shift describing the appropriate two-body scattering. T_{l_r} was parametrized by a product K-matrix resonance form, which has been discussed in detail elsewhere.[22]

The normalization integrals R were so chosen that the contribution of each partial wave to the reaction cross section of a given charge channel is given by

$$\sigma_{n_\gamma} = \pi\lambda^2(J+\tfrac{1}{2})\,|\,A_{n_\gamma}\,|^2 C_{n_\gamma}^2 .$$ (3.6)

The required integrals are

$$R^2 = \tfrac{1}{32}(m_N/W)^2[Q/(2\pi)^6][1/(2l_r+1)]$$

$$\times \int |\,T_{l_r}\,|^2(q_\gamma)^{-(2l_r+1)}p_\gamma[W_\gamma B_{l_f}(p_\gamma)]^2 dW_\gamma ,$$ (3.7)

where $\vec{Q}$ is the incident pion momentum. Since the basis functions for waves of the same J^P are not strictly orthogonal except in the zero-width limit, the total reaction cross sections also involve interference terms which cannot be ignored. Past analyses have customarily evaluated these terms numerically by generating several thousand Monte Carlo events in the four-dimensional phase space. It has been shown that these interference terms can be simply expressed in terms of overlap functions that only require integrations over two subenergy variables.[22] For the present analysis, these overlap functions were calculated efficiently and accurately using Simpson's rule and stored for later use. The interference terms determined from this procedure were also compared with Monte Carlo calculations as a program check.

IV. FITTING PROCEDURE

A maximum-likelihood procedure was chosen to fit the data. Such a procedure is the optimum method of exploiting correlations that exist in data with limited statistics. We minimized $\chi^2 = -2\ln L$, where L is the product of charge-channel likelihoods for measuring N events with differential cross sections σ_i ($i = 1, \ldots, N$) and reaction cross sections σ. χ^2 is minimized with respect to the A_{n_γ} in Eq. (3.1). The contribution to χ^2 from a single charge channel is given by

$$\chi^2 = 2N(\ln\sigma + \sigma_T/\sigma) - 2\sum_i \ln\sigma_i$$ (4.1)

with N the number of fitted events, σ_T the theoretical cross section predicted from Eq. (3.1), and σ_i the differential cross section at the ith data point given by $\sigma_i = |\,T(\omega_i)\,|^2$. The symbol ω_i denotes the four kinematic variables necessary for describing the ith event, which we chose to be W_1, W_2, $\cos\theta$, and $\cos\phi$, as defined in Fig. 1. In most cases, σ was taken to be the experimental reaction cross section. However, for $\pi^+ p \rightarrow \pi^+\pi^+ n$ above 1700 MeV, σ was taken to be σ_T because the reaction cross section was poorly determined from experiment. The experimental reaction cross sections σ_x required at each energy were obtained by fitting actual measurements[9–11,23] using the method of least squares. For each charge channel, the cross section was parametrized by a sum of resonance terms similar to those used by VerWest and Arndt in their parametrizations of NN single-pion production cross sections.[24]

A. Partial-wave constraints

Since elastic phase-shift analyses (EPSA) determine upper bounds for the inelastic partial-wave cross sections, we allowed for inclusion of a χ^2-like term in Eq. (4.1) to constrain the fitted inelastic partial-wave cross sections. This term can be written as
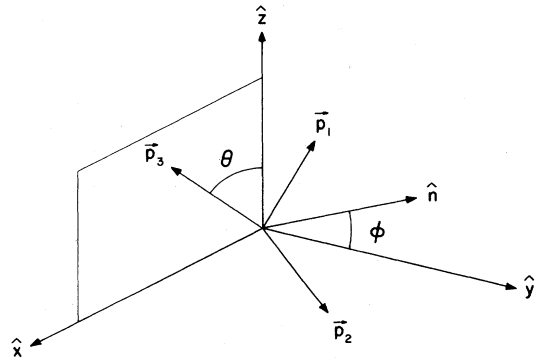

FIG. 1. The coordinate system for $\pi N \rightarrow \pi\pi N$. The momentum of the initial nucleon defines the $+z$ axis and the momentum $\vec{p}_3$ of the final-state nucleon defines the x-z plane. $\vec{p}_1$ and $\vec{p}_2$ are the momenta of the final-state pions and $\hat{n} = (\vec{p}_1 \times \vec{p}_2)/|\,\vec{p}_1 \times \vec{p}_2\,|$.

$$\chi^2_{\text{EPSA}} = \sum_{l_i, I, J} \{ [\sigma_T(l_i, 2I, 2J) - \sigma_x(l_i, 2I, 2J)] / \Delta\sigma_x(l_i, 2I, 2J) \}^2 \theta(\sigma_T(l_i, 2I, 2J) - \sigma_x(l_i, 2I, 2J)) , \qquad (4.2)$$

where $\sigma_T(l_i, 2I, 2J)$ are the fitted inelastic partial-wave cross sections, $\sigma_x(l_i, 2I, 2J)$ are the experimental values determined from EPSA with errors $\Delta\sigma_x(l_i, 2I, 2J)$, and θ is a step function to ensure that amplitudes were constrained only when the unitary bounds determined from EPSA were exceeded. In several cases, EPSA are somewhat inconsistent in their determinations of the inelastic partial-wave cross sections[25,26] and, for most energies, we had sufficient data for our fits to satisfy unitarity bounds without need of constraints. Thus, after initially fitting the entire data set, we abandoned these constraints.

B. Search algorithm

The minimization algorithm we used is a standard one in which χ^2 is first expanded to second order in the parameter increments

$$\chi^2 \simeq \chi_0^2 + \beta^T \Delta P + \tfrac{1}{2} \Delta P^T \alpha \, \Delta P . \qquad (4.3)$$

We use a vector notation in which β^T is the transpose of β. The quantity ΔP_k is the change in the kth parameter. $\beta_k = -\partial\chi^2/\partial P_k$ is the kth component of the gradient and $\alpha_{jk} = \partial^2\chi^2/\partial P_j \partial P_k$ is the second-derivative matrix. The change in parameters that minimizes the approximate χ^2 is $\Delta P_{\min} = -\alpha^{-1}\beta$. Parameters are iterated until convergence $(\beta \to 0)$. Parameter errors are obtained from the diagonal elements of the variance-covariance matrix, $E = 2\alpha^{-1}$.

We used a procedure suggested by the Berkeley-SLAC group for inverting α.[1] The second-derivative matrix is first expanded in terms of its orthonormal eigenvectors:

$$\alpha = \sum_k \lambda_k v_k v_k^T , \qquad (4.4)$$

$$v_j^T v_k = \delta_{jk} . \qquad (4.5)$$

Here, λ_k is the eigenvalue associated with eigenvector v_k:

$$\alpha v_k = \lambda_k v_k . \qquad (4.6)$$

When α is nonsingular, one has

$$\alpha^{-1} = \sum_k \lambda_k^{-1} v_k v_k^T . \qquad (4.7)$$

When α is singular, one or more eigenvalues are zero. This condition arises if there are redundant parameters. In that case, we merely inverted the nonsingular part of α. That is, only those terms with $\lambda_k > 0$ could contribute to the sum in Eq. (4.7) and hence to the step towards $\chi^2_{\min}$. This procedure also ensures that α^{-1} is a positive-definite matrix.

Rather than calculate α exactly, which is very time consuming, we instead developed an approximation for α. The contribution to the exact second-derivative matrix from a single charge channel is given by

$$\alpha_{jk} = 2N[\sigma_{T,jk}/\sigma - (\sigma_{T,j}\sigma_k)/\sigma^2] \\ - 2\sum_i [\sigma_{i,jk}/\sigma_i - (\sigma_{i,j}\sigma_{i,k})/\sigma_i^2] , \qquad (4.8)$$

where

$$\sigma_{T,j} = \partial\sigma_T/\partial P_j , \qquad (4.9\text{a})$$

$$\sigma_{T,jk} = \partial^2\sigma_T/\partial P_j \partial P_k , \qquad (4.9\text{b})$$

$$\sigma_{i,j} = \partial\sigma_i/\partial P_j , \qquad (4.9\text{c})$$

$$\sigma_{i,jk} = \partial^2\sigma_i/\partial P_j \partial P_k , \qquad (4.9\text{d})$$

$$\sigma_k = \partial\sigma/\partial P_k . \qquad (4.9\text{e})$$

For large numbers of events,

$$\sum_i (\sigma_{i,jk}/\sigma_i) \simeq N(\sigma_{T,jk}/\sigma_T) ,$$

from which we obtain the approximate second-derivative matrix

$$\alpha_{jk} \simeq 2N(1/\sigma - 1/\sigma_T)\sigma_{T,jk} - 2N(\sigma_{T,j}\sigma_k)/\sigma^2 \\ + 2\sum_i (\sigma_{i,j}\sigma_{i,k})/\sigma_i^2 . \qquad (4.10)$$

V. ANALYSIS PROCEDURE

We limited our analysis to those partial waves with $J \leq \frac{7}{2}$, $l_i \leq 4$, and $l_f \leq 4$. Studies of elastic πN scattering indicate that higher partial waves have negligible inelasticity below 1600 MeV, where the only important inelastic channels are $\pi N \to \eta N$ and $\pi N \to \pi\pi N$. Other inelastic reactions become important above 1600 MeV as shown in Fig. 2, which displays the total πN inelastic isospin cross sections deduced from elastic partial-wave analyses[25,26] and their single-pion-production components deduced from the least-squares fits discussed earlier. Inelasticity in higher partial waves above 1600 MeV is thought to be strongly associated with the opening of these other inelastic channels.

For the quasi-two-body channels $\pi\Delta$, ρN, ϵN, and $\pi N^*(P_{11})$, the above criteria for choosing partial waves result in a total of 92 amplitudes which are listed in Table III. The amplitudes are denoted by the standard convention $(l_i, l_f, 2I, 2J)$ followed by the isobar and spectator. ρN amplitudes carry a subscript 1 or 3 to denote the total spin ($\frac{1}{2}$ or $\frac{3}{2}$) of the ρ and final-state nucleon.

The large number of parameters and the relatively small amount of data available at any given energy prohibit a meaningful simultaneous fit of all 92 amplitudes. Since waves with high orbital angular momenta are suppressed at lower energies, they can usually be neglected. Because of this simplification, we started our analysis at the lower energies and worked upward. $\pi N \to \pi N^*$ amplitudes were not searched in the initial low-energy fits since πN^* channels are effectively closed below about 1500 MeV.
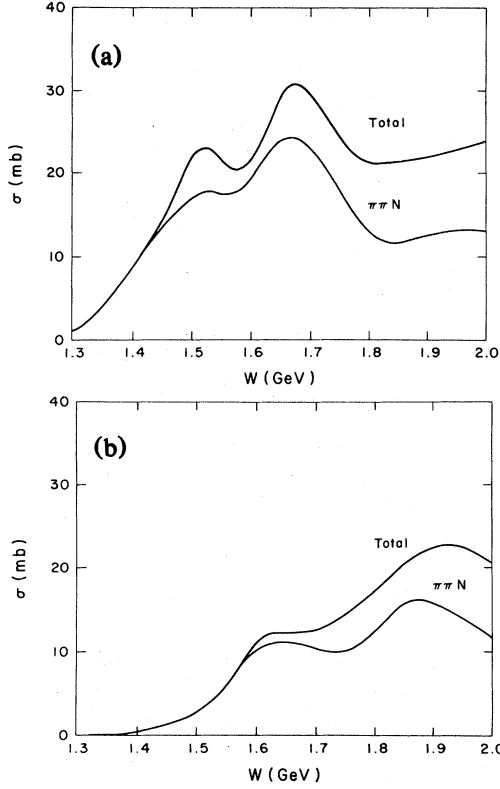
FIG. 2. (a) The total πN inelastic cross section for $I = \frac{1}{2}$ and the component from single-pion production. The bump in the total cross section near 1500 MeV is from the $S_{11}(1535)$ resonance contribution to $\pi^- p \to \eta n$. (b) The total πN inelastic cross section for $I = \frac{3}{2}$ and the component from single-pion production.

A. Preliminary analysis

We began by searching for solutions at 1440 MeV where over 5000 events were available. Only amplitudes for the P_{11}, D_{13}, and D_{33} partial waves were searched since EPSA predict other partial waves at this energy to have inelastic partial-wave cross sections under 1 mb.[25,26] From the five possible $I = \frac{3}{2}$ amplitudes, we retained only $DS33(\pi\Delta)$. Three of the neglected $I = \frac{3}{2}$ amplitudes have $l_f = 2$ and should therefore be small. The other neglected amplitude is $DS33(\rho_3 N)$, which we expect to be small compared to $DS33(\pi\Delta)$ at this energy. This left 11 amplitudes to be determined. Unitarity requires that the inelastic D_{13} and D_{33} amplitudes be nearly real just above threshold since the elastic D_{13} and D_{33} amplitudes are nearly real in this energy range. We therefore restricted the inelastic D_{13} and D_{33} amplitudes to be real. Thus, only 15 parameters remained to be searched. Initial values of the free parameters were randomly generated within the unitary circle. With these kinds of assumptions, solutions were generated from about 75 random starts. Although several different solutions were obtained, χ^2 for the best solution was 202 smaller than χ^2 for the second best. Consequently, we interpreted our best solution to be the unique "correct" solution, which made it possible to extend our analysis to higher and lower energies by requiring continuous variation in energy of the well-determined parameters.

With a unique solution with which to join at 1440 MeV, we began a systematic search for the important amplitudes. The importance of each amplitude was judged by two factors: (1) its size as measured by its modulus $|A|$ and (2) how well it was determined as measured by its fractional error $\Delta|A|/|A|$. Specifically, we were

TABLE III. The 92 amplitudes for quasi-two-body channels $\pi\Delta$, ρN, ϵN, and $\pi N^*(P_{11})$ with $J \leq \frac{7}{2}$, $l_i \leq 4$, and $l_f \leq 4$.

$SD\,11(\pi\Delta)$	$SD\,31(\pi\Delta)$	$SD\,11(\rho_3 N)$	$SD\,31(\rho_3 N)$
$PP\,11(\pi\Delta)$	$PP\,31(\pi\Delta)$	$PP\,11(\rho_3 N)$	$PP\,31(\rho_3 N)$
$DS\,13(\pi\Delta)$	$DS\,33(\pi\Delta)$	$DS\,13(\rho_3 N)$	$DS\,33(\rho_3 N)$
$DD\,13(\pi\Delta)$	$DD\,33(\pi\Delta)$	$DD\,13(\rho_3 N)$	$DD\,33(\rho_3 N)$
$PP\,13(\pi\Delta)$	$PP\,33(\pi\Delta)$	$PP\,13(\rho_3 N)$	$PP\,33(\rho_3 N)$
$PF\,13(\pi\Delta)$	$PF\,33(\pi\Delta)$	$PF\,13(\rho_3 N)$	$PF\,33(\rho_3 N)$
$DD\,15(\pi\Delta)$	$DD\,35(\pi\Delta)$	$DD\,15(\rho_3 N)$	$DD\,35(\rho_3 N)$
$DG\,15(\pi\Delta)$	$DG\,35(\pi\Delta)$	$DG\,15(\rho_3 N)$	$DG\,35(\rho_3 N)$
$FP\,15(\pi\Delta)$	$FP\,35(\pi\Delta)$	$FP\,15(\rho_3 N)$	$FP\,35(\rho_3 N)$
$FF\,15(\pi\Delta)$	$FF\,35(\pi\Delta)$	$FF\,15(\rho_3 N)$	$FF\,35(\rho_3 N)$
$GD\,17(\pi\Delta)$	$GD\,37(\pi\Delta)$	$GD\,17(\rho_3 N)$	$GD\,37(\rho_3 N)$
$GG\,17(\pi\Delta)$	$GG\,37(\pi\Delta)$	$GG\,17(\rho_3 N)$	$GG\,37(\rho_3 N)$
$FF\,17(\pi\Delta)$	$FF\,37(\pi\Delta)$	$FF\,17(\rho_3 N)$	$FF\,37(\rho_3 N)$
$SS\,11(\pi N^*)$	$SS\,31(\pi N^*)$	$SS\,11(\rho_1 N)$	$SS\,31(\rho_1 N)$
$PP\,11(\pi N^*)$	$PP\,31(\pi N^*)$	$PP\,11(\rho_1 N)$	$PP\,31(\rho_1 N)$
$DD\,13(\pi N^*)$	$DD\,33(\pi N^*)$	$DD\,13(\rho_1 N)$	$DD\,33(\rho_1 N)$
$PP\,13(\pi N^*)$	$PP\,33(\pi N^*)$	$PP\,13(\rho_1 N)$	$PP\,33(\rho_1 N)$
$DD\,15(\pi N^*)$	$DD\,35(\pi N^*)$	$DD\,15(\rho_1 N)$	$DD\,35(\rho_1 N)$
$FF\,15(\pi N^*)$	$FF\,35(\pi N^*)$	$FF\,15(\rho_1 N)$	$FF\,35(\rho_1 N)$
$GG\,17(\pi N^*)$	$GG\,37(\pi N^*)$	$GG\,17(\rho_1 N)$	$GG\,37(\rho_1 N)$
$FF\,17(\pi N^*)$	$FF\,37(\pi N^*)$	$FF\,17(\rho_1 N)$	$FF\,37(\rho_1 N)$
$SP\,11(\epsilon N)$	$DP\,13(\epsilon N)$	$DF\,15(\epsilon N)$	$GF\,17(\epsilon N)$
$PS\,11(\epsilon N)$	$PD\,13(\epsilon N)$	$FD\,15(\epsilon N)$	$FG\,17(\epsilon N)$

sensitive to amplitudes which satisfied the conditions $|A| \geq 0.08 \ (J+\frac{1}{2})^{-1/2}$ and $|A|/\Delta|A| \geq 3$. For each amplitude we calculated an "importance parameter" given by

$$M = [\ |A|/(3\Delta|A|)]\{ \ |A|/[0.08(J+\tfrac{1}{2})^{-1/2}] \} \ . \quad (5.1)$$

Those amplitudes with $M < 1$ were small and unnecessary for a good fit whereas those with $M > 10$ were quite important. We then refitted the data at 1440 MeV including all 23 amplitudes for $\pi\Delta$, ϵN, and ρN with $l_i \leq 3$, $l_f(\pi\Delta) \leq 2$, $l_f(\epsilon N) \leq 2$, and $l_f(\rho N) = 0$. The overall phase was determined by requiring $DS33 \ (\pi\Delta)$ to be real. For those amplitudes that had $M > 10$ in the original solution, initial values were generated randomly within a domain of two standard deviations of their earlier fitted values. Initial values for less important amplitudes were generated completely randomly within the unitary circle. This procedure for generating solutions was repeated on the order of 10 times at each energy, occasionally, with slightly different distinctions between the important and less important amplitudes.

After obtaining a 23-wave solution at 1440 MeV, we selected amplitudes with $M > 10$ to generate, as discussed above, initial values at 1460 MeV. This procedure for generating initial values was repeated to obtain solutions at higher energies. At 1600 MeV, we introduced amplitudes for the $\pi N^*(P_{11})$ channel and extended our search to include a total of 47 amplitudes satisfying $l_i \leq 4$, $l_f(\pi\Delta) \leq 3$, $l_f(\epsilon N) \leq 3$, $l_f(\rho N) \leq 1$, and $l_f(\pi N^*) \leq 1$. No F_{17} or G_{37} waves were searched since EPSA predict negligible inelasticity in these waves below about 1750 MeV.[25,26] At 1620 MeV, only $\pi^+ p$ events were fitted since there were too few $\pi^- p$ events to determine the $I = \frac{1}{2}$ amplitudes.

At 1700 MeV, we extended our search to include a total of 76 amplitudes satisfying $l_i \leq 4$, $l_f(\pi\Delta) \leq 4$, $l_f(\epsilon N) \leq 4$, $l_f(\rho N) \leq 3$, and $l_f(\pi N^*) \leq 3$. Again, no F_{17} or G_{37} waves were searched. At this point in our analysis, the majority of waves searched were small rather than large. To decrease the influence of "noise" waves, we generated three slightly different solutions with the total number of waves in each restricted never to exceed 50. For each solution, we searched the set of waves determined to be important at the adjacent lower energy and a different subset of less important waves. This procedure of generating three solutions at each energy was continued for higher energies. At 1725 MeV, we searched all waves with $l_i \leq 4$ and $l_f \leq 4$ except for F_{17} waves, which were added at 1755 MeV, and G_{37} waves, which were added at 1870 MeV. Unfortunately, above 1725 MeV, the number of events available for our analysis became insufficient to reliably determine completely unique solutions. Below this energy, our requirement of energy continuity for the major amplitudes produced a single continuous solution from the lower energies. Above 1725 MeV, the solution split into two chains, mainly because of lack of data in the $\pi^+ p \rightarrow \pi^+ \pi^+ n$ channel. We selected the chain which produced the lowest X^2 at 1870 MeV, where over half the data are $\pi^+ p$ events (mostly $\pi^+ p \rightarrow \pi^0 \pi^+ p$). In the rejected chain, the P_{33} cross section is negligible at high energies as in the Berkeley-SLAC solution.[1] Waves with

$J > \frac{3}{2}$ were essentially the same for both chains.

Our procedure for generating solutions above 1440 MeV was also used to extend the analysis to lower energies. The process was simplified because of the suppression of waves with high orbital angular momenta. By 1400 MeV, f waves were no longer important so our search included only the 20 waves with $l_i \leq 2$, $l_f(\pi\Delta) \leq 2$, $l_f(\epsilon N) \leq 2$, and $l_f(\rho N) = 0$. At 1340 and 1375 MeV, we searched only the 13 waves with $l_i \leq 2$, $l_f(\pi\Delta) \leq 1$, $l_f(\epsilon N) \leq 1$, and $l_f(\rho N) = 0$.

B. Final analysis

After completing the above preliminary analysis, we reanalyzed the data using a reduced set of waves discussed below. Since some waves were found to be rather large when first searched, it was necessary to repeat the analysis with their inclusion at lower energies. We began reanalysis at 1790 MeV with a reduced set of waves and worked upward generating solutions as before. We also generated solutions working downward in energy, removing waves as they became unimportant to the fit (i.e., when $M < 1$).

The following procedure was used to select the reduced set of waves. For each wave in Table III, we first tabulated the fitted amplitudes and their associated importance parameters at each energy. We retained every amplitude which had $M \geq 10$ at four or more energies. The following 26 waves met this requirement: $PP11(\pi\Delta)$, $DS13(\pi\Delta)$, $DD13(\pi\Delta)$, $DD15(\pi\Delta)$, $FP15(\pi\Delta)$, $SD31(\pi\Delta)$, $DS33(\pi\Delta)$, $PP33(\pi\Delta)$, $FF35(\pi\Delta)$, $FF37(\pi\Delta)$, $SP11(\epsilon N)$, $PS11(\epsilon N)$, $DP13(\epsilon N)$, $FD15(\epsilon N)$, $DS13(\rho_3 N)$, $DD15(\rho_3 N)$, $FP15(\rho_3 N)$, $GD17(\rho_3 N)$, $DS33(\rho_3 N)$, $FP35(\rho_3 N)$, $SS11(\rho_1 N)$, $PP13(\rho_1 N)$, $SS31(\rho_1 N)$, $SS11(\pi N^*)$, $SS31(\pi N^*)$, and $PP33(\pi N^*)$. All 13 waves with $l_f = 4$ and the 8 additional πN^* waves with $l_f \geq 2$ were found to be unimportant and were eliminated. We also eliminated the following 17 waves which behaved discontinuously and were small $(M \leq 5)$ over the entire energy range: $PF13(\pi\Delta)$, $FF17(\pi\Delta)$, $PF33(\pi\Delta)$, $GD37(\pi\Delta)$, $PP11(\rho_3 N)$, $PF13(\rho_3 N)$, $FF17(\rho_3 N)$, $DD33(\rho_3 N)$, $PF33(\rho_3 N)$, $FF35(\rho_3 N)$, $GD37(\rho_3 N)$, $FF15(\rho_1 N)$, $FF17(\rho_1 N)$, $DD33(\rho_1 N)$, $DD35(\rho_1 N)$, $FF35(\rho_1 N)$, and $FF37(\rho_1 N)$. The 28 waves that remained were either moderately or negligibly small $(5 < M < 10)$ over the entire energy range.

After solutions had been generated at all energies with the reduced set of waves, we again applied our criteria for keeping or eliminating waves. We kept five waves: $SD11(\pi\Delta)$, $SD11(\rho_3 N)$, $SD31(\rho_3 N)$, $PP11(\rho_1 N)$, and $PP31(\pi N^*)$ and eliminated 18: $PP13(\pi\Delta)$, $GD17(\pi\Delta)$, $PP31(\pi\Delta)$, $DD35(\pi\Delta)$, $PD13(\epsilon N)$, $DF15(\epsilon N)$, $GF17(\epsilon N)$, $PP13(\rho_3 N)$, $DD13(\rho_3 N)$, $PP31(\rho_3 N)$, $PP33(\rho_3 N)$, $DD35(\rho_3 N)$, $FF37(\rho_3 N)$, $DD13(\rho_1 N)$, $PP31(\rho_1 N)$, $PP33(\rho_1 N)$, $PP11(\pi N^*)$, and $PP13(\pi N^*)$. Our final set of 36 waves is summarized in Table IV. For the final stage of the reanalysis, we generated solutions at each energy using the final set of 36 waves and our standard procedure discussed above. We decided not to include any πN^* channels in our final analysis except the $\pi N^*(P_{11})$, since other πN^* channels were found to be relatively unimportant, as discussed below.

TABLE IV. Final set of 36 amplitudes included in the analysis. The energy (in MeV) at which each amplitude was first included is also given.

$SP\,11(\epsilon N)$	1480	$SS\,31(\rho_1 N)$	1400
$SS\,11(\rho_1 N)$	1400	$SD\,31(\rho_3 N)$	1565
$SD\,11(\rho_3 N)$	1565	$SD\,31(\pi\Delta)$	1460
$SD\,11(\pi\Delta)$	1565	$SS\,31(\pi N^*)$	1640
$SS\,11(\pi N^*)$	1595	$PP\,31(\pi N^*)$	1660
$PS\,11(\epsilon N)$	1340	$PP\,33(\pi\Delta)$	1460
$PP\,11(\rho_1 N)$	1680	$PP\,33(\pi N^*)$	1480
$PP\,11(\pi\Delta)$	1340	$DS\,33(\rho_3 N)$	1400
$PP\,13(\rho_1 N)$	1640	$DS\,33(\pi\Delta)$	1340
$DP\,13(\epsilon N)$	1340	$DD\,33(\pi\Delta)$	1400
$DS\,13(\rho_3 N)$	1340	$FP\,35(\rho_3 N)$	1565
$DS\,13(\pi\Delta)$	1340	$FP\,35(\pi\Delta)$	1565
$DD\,13(\pi\Delta)$	1400	$FF\,35(\pi\Delta)$	1595
$DD\,15(\rho_1 N)$	1595	$FF\,37(\pi\Delta)$	1565
$DD\,15(\rho_3 N)$	1595		
$DD\,15(\pi\Delta)$	1400		
$FD\,15(\epsilon N)$	1480		
$FP\,15(\rho_3 N)$	1480		
$FF\,15(\rho_3 N)$	1640		
$FP\,15(\pi\Delta)$	1480		
$FF\,15(\pi\Delta)$	1640		
$GD\,17(\rho_3 N)$	1680		

C. Omitted decay channels

It has been suggested that several πN^* channels may contribute to single-pion production below 2000 MeV.[1-3,27] Our analysis is the first to investigate, within an isobar model, the importance of πN^* channels other than $\pi N^*(P_{11})$. We chose to study the channels $\pi N^*(S_{11})$, $\pi N^*(D_{13})$, and $\pi N^*(F_{15})$ because of the relatively low masses of their N^*'s and because of their large elastic branching fractions.[28] Each new channel was studied separately by generating solutions at 1700 MeV and working higher in energy. The πN^* amplitudes with $l_f \leq 1$ were fitted simultaneously with the final reduced set of waves discussed above. Table V summarizes the new πN^* amplitudes investigated for each channel.

Of the 22 new πN^* amplitudes fitted, 12 were found to be negligible over the entire energy range: $PS\,31(\pi S_{11})$,

TABLE V. The 22 amplitudes for quasi-two-body channels $\pi N^*(S_{11})$, $\pi N^*(D_{13})$, and $\pi N^*(F_{15})$ with $J \leq \frac{7}{2}$, $l_i \leq 4$, and $l_f \leq 1$.

$SP\,11(\pi S_{11})$	$SP\,31(\pi S_{11})$
$PS\,11(\pi S_{11})$	$PS\,31(\pi S_{11})$
$DP\,13(\pi S_{11})$	$DP\,33(\pi S_{11})$
$SP\,11(\pi D_{13})$	$SP\,31(\pi D_{13})$
$PS\,13(\pi D_{13})$	$PS\,33(\pi D_{13})$
$DP\,13(\pi D_{13})$	$DP\,33(\pi D_{13})$
$DP\,15(\pi D_{13})$	$DP\,35(\pi D_{13})$
$PP\,13(\pi F_{15})$	$PP\,33(\pi F_{15})$
$DS\,15(\pi F_{15})$	$DS\,35(\pi F_{15})$
$FP\,15(\pi F_{15})$	$FP\,35(\pi F_{15})$
$FP\,17(\pi F_{15})$	$FP\,37(\pi F_{15})$

$DP\,33(\pi S_{11})$, $PS\,13(\pi D_{13})$, $DP\,13(\pi D_{13})$, $PS\,33(\pi D_{13})$, $DP\,33(\pi D_{13})$, $DP\,35(\pi D_{13})$, $DS\,15(\pi F_{15})$, $FP\,17(\pi F_{15})$, $PP\,33(\pi F_{15})$, $DS\,35(\pi F_{15})$, and $FP\,35(\pi F_{15})$. We found the $D_{15}(1675)$ resonance to couple significantly to $DP\,15(\pi D_{13})$ with $(xx')^{1/2} \simeq -0.15$, where x is the elastic branching fraction and x' is the appropriate inelastic branching fraction. The sign of the coupling is expressed according to the "baryon-first" phase convention discussed in the following section. We also found the $F_{37}(1950)$ resonance to couple significantly to $FP\,37(\pi F_{15})$ with $(xx')^{1/2} \simeq +0.20$. It is difficult to judge the importance of the πS_{11} amplitudes since they generally tended to be highly correlated with other amplitudes, notably those for the ϵN channel.

VI. DISCUSSION OF RESULTS

In the first part of this section, we discuss the features of our analysis that are independent of the overall phase of the solutions at each energy. In the second part, we present our first attempts at resolving the overall phase ambiguity by comparing phases of resonant elastic and inelastic amplitudes and performing a constrained "minimum-path" analysis.

A. Partial-wave cross sections

In Fig. 3, we display our results for the inelastic partial-wave cross sections determined at each energy from our preferred solutions and, for comparison, the results of two fairly recent analyses of πN elastic scattering.[25,26] Numerical values for our results are presented in Table VI. The contributions of individual waves to the inelastic partial-wave cross sections are shown in Fig. 4. The following discussion summarizes the principal features of each partial wave. Masses of established resonances are those assigned by the Particle Data Group.[28]

S_{11}. The $S_{11}(1535)$ is observed decaying into the ρN and ϵN channels. About 80% of the expected inelasticity is unobserved because of the dominant ηN decay mode. We account for virtually all of the inelasticity associated with decay of the $S_{11}(1650)$ with $\pi\Delta$ and ρN its major decay channels. We possibly observe a higher-mass S_{11} decaying into ϵN, ρN, and $\pi N^*(P_{11})$.

P_{11}. We observe the $P_{11}(1440)$ to have large $\pi\Delta$ and ϵN decays that account for practically all of its inelasticity. We account for about a third of the expected inelasticity for the $P_{11}(1710)$ with $\pi\Delta$ its major $\pi\pi N$ decay channel. Most of its unobserved inelasticity may be accounted for by its decays into ηN, $K\Lambda$, and $K\Sigma$.[28] It may also have a significant decay into ωN. Our analysis also suggests a possible P_{11} near 1900 MeV with $\pi\Delta$ and ρN the dominant $\pi\pi N$ channels.

P_{13}. We see no clear evidence for the $P_{13}(1540)$ or $P_{13}(1710)$. Instead, the observed inelasticity seems to be mainly associated with the ρN decay of a resonance near 1850 MeV. We suggest that ωN may be the major inelastic decay channel for the unobserved $P_{13}(1710)$.

D_{13}. Our analysis accounts for virtually all of the D_{13} inelasticity. The $D_{13}(1520)$ is clearly observed decaying into $\pi\Delta$ and ρN with the latter decay mode dominant. We observe the $D_{13}(1700)$ less clearly decaying into $\pi\Delta$,
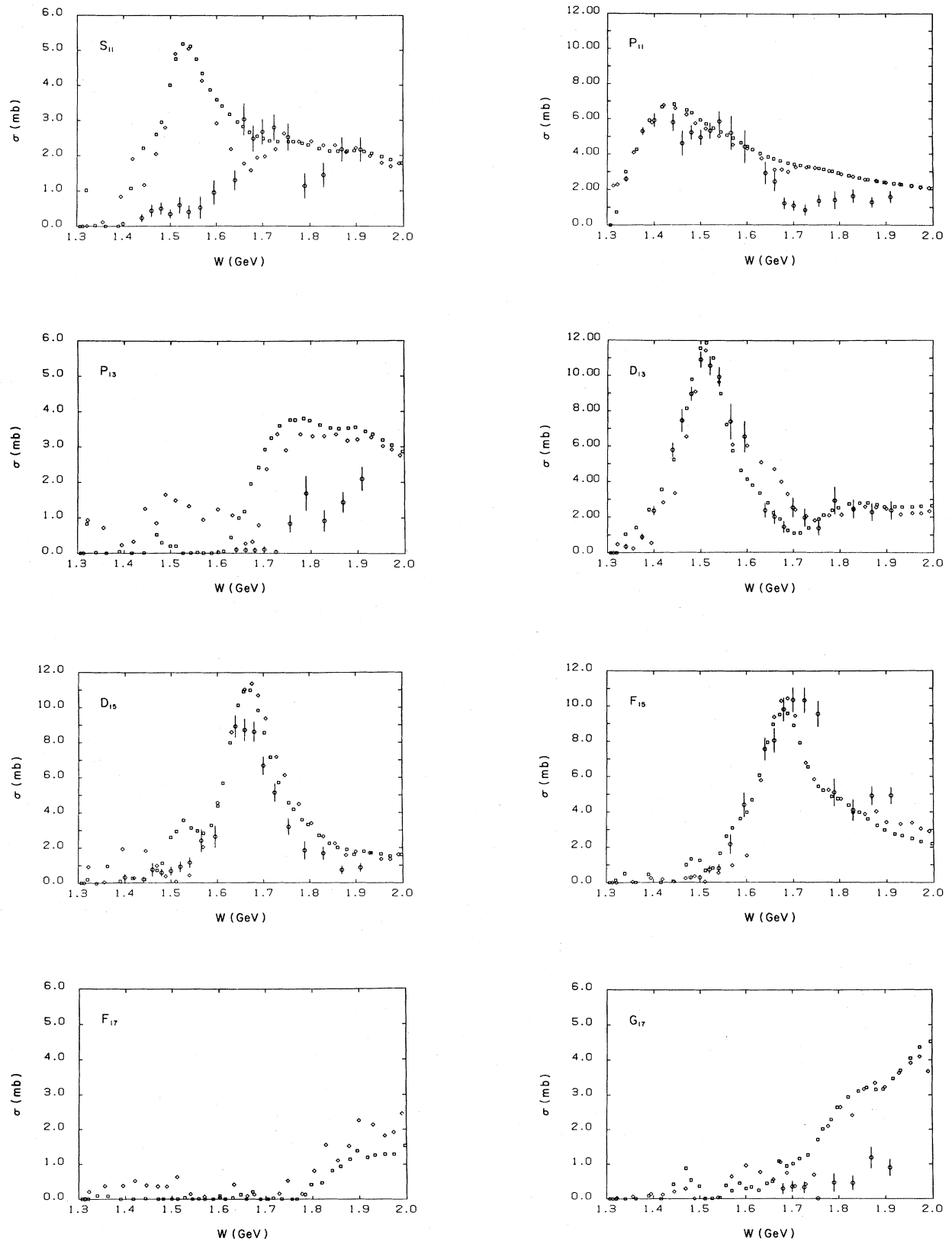
FIG. 3. Inelastic partial-wave cross sections. The results of the present work are indicated by circles and the predictions of EPSA are indicated by boxes (Ref. 25) and diamonds (Ref. 26). Displayed errors in the results of the present work are twice as large as those obtained from our fitting algorithm.
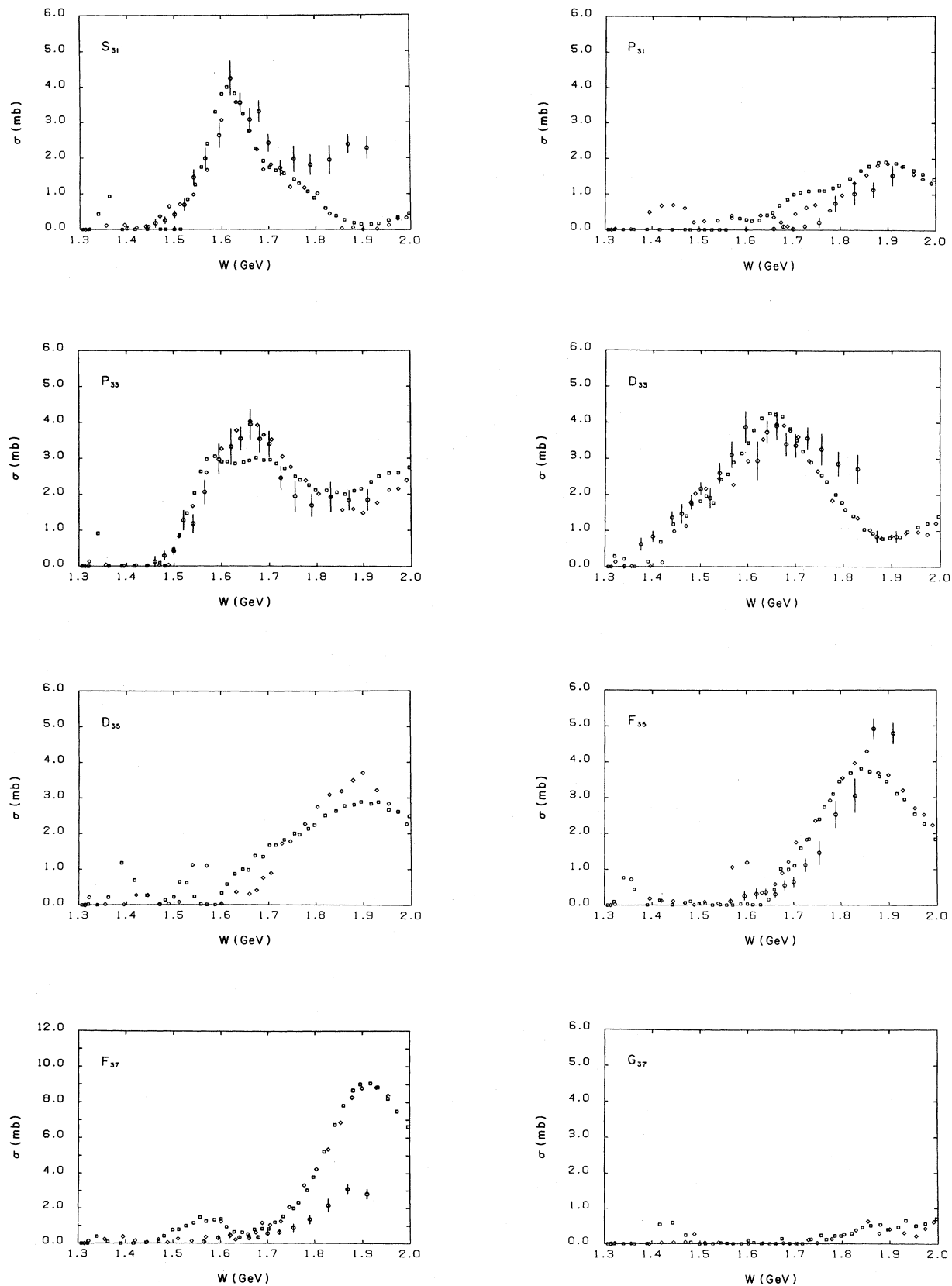
FIG. 3. *(Continued.)*

TABLE VI. Inelastic partial-wave cross sections (in mb) determined from this analysis.

W (MeV)	S_{11}	P_{11}	P_{13}
1340		2.60±0.08	
1375		5.31±0.11	
1400	0.07±0.02	5.93±0.19	
1440	0.23±0.05	5.82±0.24	
1460	0.43±0.08	4.63±0.35	
1480	0.50±0.08	5.24±0.20	
1500	0.34±0.06	4.96±0.21	
1520	0.59±0.11	5.34±0.22	
1540	0.40±0.09	5.86±0.27	
1565	0.52±0.15	5.21±0.48	
1595	0.95±0.17	4.43±0.46	
1620			
1640	1.30±0.14	2.93±0.31	0.10±0.04
1660	3.03±0.23	2.45±0.27	0.09±0.04
1680	2.48±0.19	1.23±0.16	0.08±0.03
1700	2.67±0.18	1.08±0.14	0.11±0.04
1725	2.80±0.19	0.83±0.15	0.04±0.03
1755	2.52±0.19	1.36±0.17	0.84±0.12
1790	1.14±0.17	1.40±0.25	1.69±0.24
1830	1.44±0.17	1.63±0.18	0.91±0.15
1870	2.18±0.17	1.29±0.14	1.44±0.14
1910	2.17±0.17	1.58±0.16	2.09±0.17

W (MeV)	D_{13}	D_{15}	F_{15}	G_{17}
1340	0.35±0.07			
1375	0.88±0.08			
1400	2.35±0.12	0.32±0.08		
1440	5.78±0.20	0.19±0.08		
1460	7.46±0.32	0.75±0.19		
1480	8.98±0.19	0.58±0.10	0.28±0.06	
1500	10.92±0.22	0.67±0.12	0.28±0.06	
1520	10.58±0.27	0.91±0.15	0.72±0.10	
1540	9.94±0.27	1.14±0.14	0.80±0.11	
1565	7.41±0.50	2.40±0.32	2.17±0.27	
1595	6.54±0.44	2.63±0.31	4.41±0.35	
1620				
1640	2.37±0.20	8.94±0.31	7.58±0.31	
1660	2.00±0.19	8.73±0.31	8.06±0.34	
1680	1.43±0.16	8.63±0.28	9.83±0.33	0.29±0.07
1700	2.52±0.27	6.70±0.26	10.36±0.34	0.35±0.07
1725	1.95±0.24	5.15±0.25	10.34±0.35	0.32±0.08
1755	1.36±0.20	3.20±0.24	9.57±0.36	0.01±0.01
1790	2.93±0.38	1.84±0.25	5.11±0.39	0.46±0.13
1830	2.46±0.26	1.68±0.18	4.11±0.30	0.45±0.10
1870	2.27±0.24	0.73±0.12	4.92±0.26	1.19±0.15
1910	2.38±0.25	0.87±0.12	4.93±0.23	0.90±0.12

ρN, and ϵN. The ϵN channel may also be associated with the decay of a higher mass D_{13}.

D_{15}. Our analysis accounts for almost all of the D_{15} inelasticity. The dominant inelastic decay mode of the $D_{15}(1675)$ resonance is clearly $\pi\Delta$. However, our study of πN^* decay channels indicates that it also has a significant $\pi N^*(D_{13})$ decay. Inelasticity above the $D_{15}(1675)$ resonance is mainly associated with the ρN channel.

F_{15}. All of the F_{15} inelasticity is accounted for by our analysis. The $F_{15}(1680)$ is clearly observed decaying into the $\pi\Delta$, ρN, and ϵN channels. We also observe an F_{15} near 1850 MeV with large ρN and ϵN decay modes.

F_{17}. We see no evidence for $\pi\pi N$ inelasticity in this wave.

G_{17}. About a fourth of the G_{17} inelasticity is accounted for by our analysis with ρN the only significant $\pi\pi N$ decay channel.

S_{31}. Our analysis accounts for all of the expected S_{31}

TABLE VI. (Continued).

W (MeV)	S_{31}	P_{31}	P_{33}
1340			
1375			
1400	0.03±0.02		
1440	0.07±0.03		
1460	0.17±0.06		0.13±0.07
1480	0.25±0.05		0.29±0.06
1500	0.42±0.05		0.42±0.06
1520	0.69±0.08		1.28±0.14
1540	1.46±0.11		1.18±0.13
1565	1.99±0.14		2.07±0.17
1595	2.64±0.17		2.98±0.21
1620	4.25±0.24		3.33±0.25
1640	3.57±0.13		3.56±0.16
1660	3.09±0.16	0.03±0.02	3.96±0.21
1680	3.32±0.15	0.09±0.03	3.55±0.18
1700	2.43±0.12	0.03±0.02	3.41±0.18
1725	1.73±0.11	0.10±0.03	2.46±0.17
1755	1.97±0.18	0.21±0.07	1.95±0.22
1790	1.81±0.14	0.74±0.11	1.69±0.16
1830	1.95±0.20	1.01±0.16	1.93±0.20
1870	2.39±0.13	1.12±0.11	1.84±0.14
1910	2.28±0.15	1.52±0.14	1.85±0.15

W (MeV)	D_{33}	F_{35}	F_{37}
1340	0.01±0.02		
1375	0.62±0.09		
1400	0.83±0.08		
1440	1.36±0.08		
1460	1.47±0.14		
1480	1.78±0.10		
1500	2.16±0.09		
1520	1.91±0.14		
1540	2.60±0.14		
1565	3.11±0.18	0.11±0.03	0.09±0.04
1595	3.89±0.22	0.25±0.06	0.31±0.06
1620	2.95±0.27	0.31±0.07	0.46±0.09
1640	3.75±0.16	0.36±0.05	0.33±0.05
1660	3.92±0.19	0.30±0.05	0.30±0.05
1680	3.41±0.16	0.55±0.07	0.34±0.06
1700	3.37±0.16	0.64±0.07	0.57±0.07
1725	3.58±0.15	1.12±0.09	0.64±0.07
1755	3.27±0.21	1.46±0.16	0.88±0.12
1790	2.87±0.17	2.53±0.19	1.36±0.13
1830	2.72±0.20	3.06±0.23	2.16±0.19
1870	0.84±0.08	4.92±0.14	3.10±0.13
1910	0.84±0.08	4.80±0.14	2.81±0.14

inelasticity. The $S_{31}(1620)$ is clearly observed decaying into the $\pi\Delta$ and ρN channels. In disagreement with expectations from EPSA, we find large inelasticity ($\simeq 2$ mb) above the energy range of the $S_{31}(1620)$. This inelasticity is mainly associated with the $\pi N^*(P_{11})$ channel and is probably due to decay of the $S_{31}(1900)$ resonance.

P_{31}. Our analysis accounts for virtually all of the P_{31} inelasticity with $\pi N^*(P_{11})$ the dominant decay channel. We see no clear evidence for the $P_{31}(1550)$.

P_{33}. We account for all of the expected P_{33} inelasticity and probably observe resonances at 1600 and 1900 MeV. We find the dominant $\pi\pi N$ decay mode of the 1600 MeV resonance to be $\pi\Delta$ with, however, a significant $\pi N^*(P_{11})$ decay.

D_{33}. Our analysis accounts for all of the expected D_{33} inelasticity with $\pi\Delta$ and ρN the dominant decay channels. Above 1700 MeV, our analysis finds about 1 mb more inelasticity than expected from EPSA.
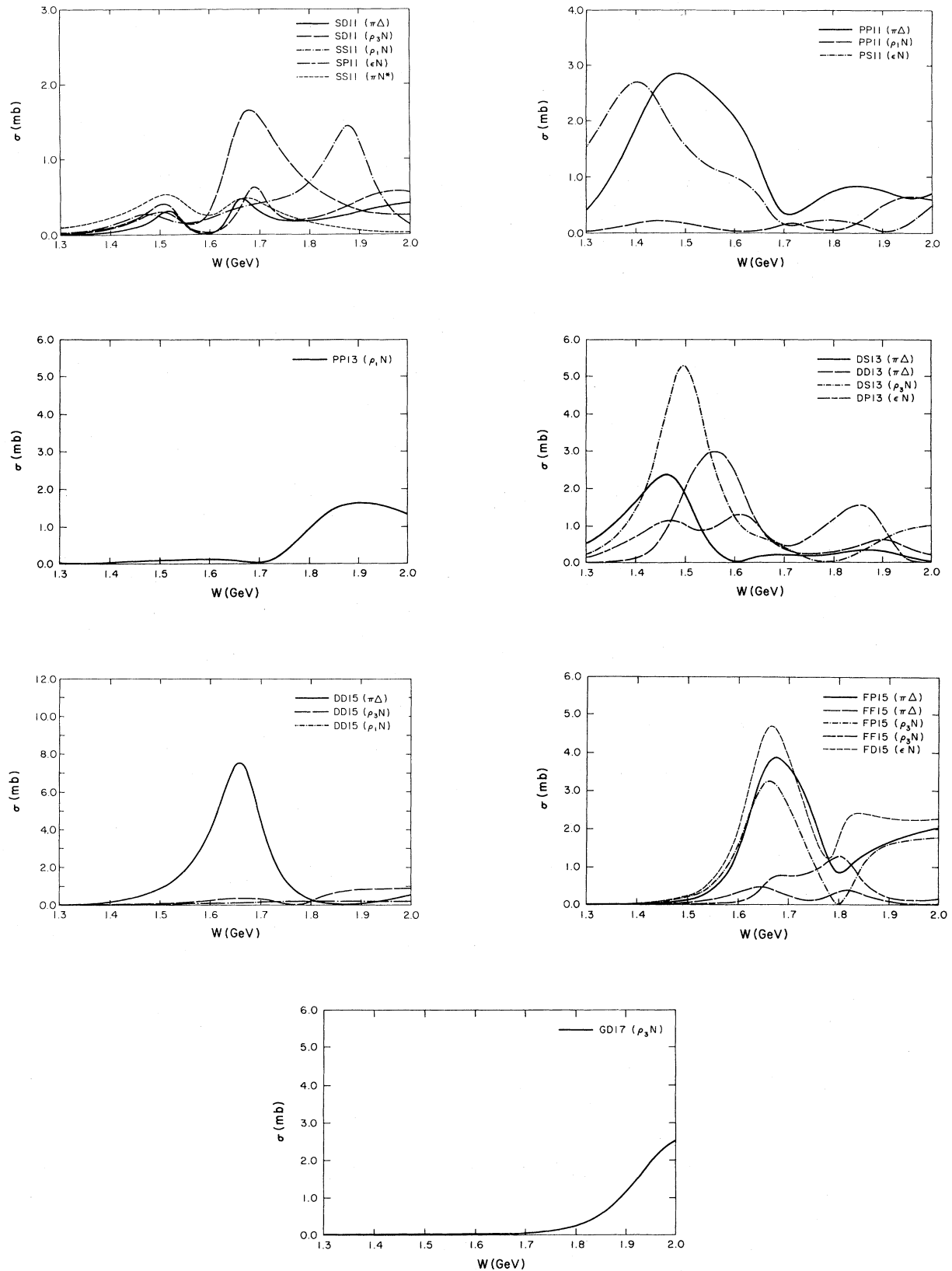
FIG. 4. The contributions of individual amplitudes to the inelastic partial-wave cross sections. The curves were obtained from energy-dependent fits of the amplitudes.
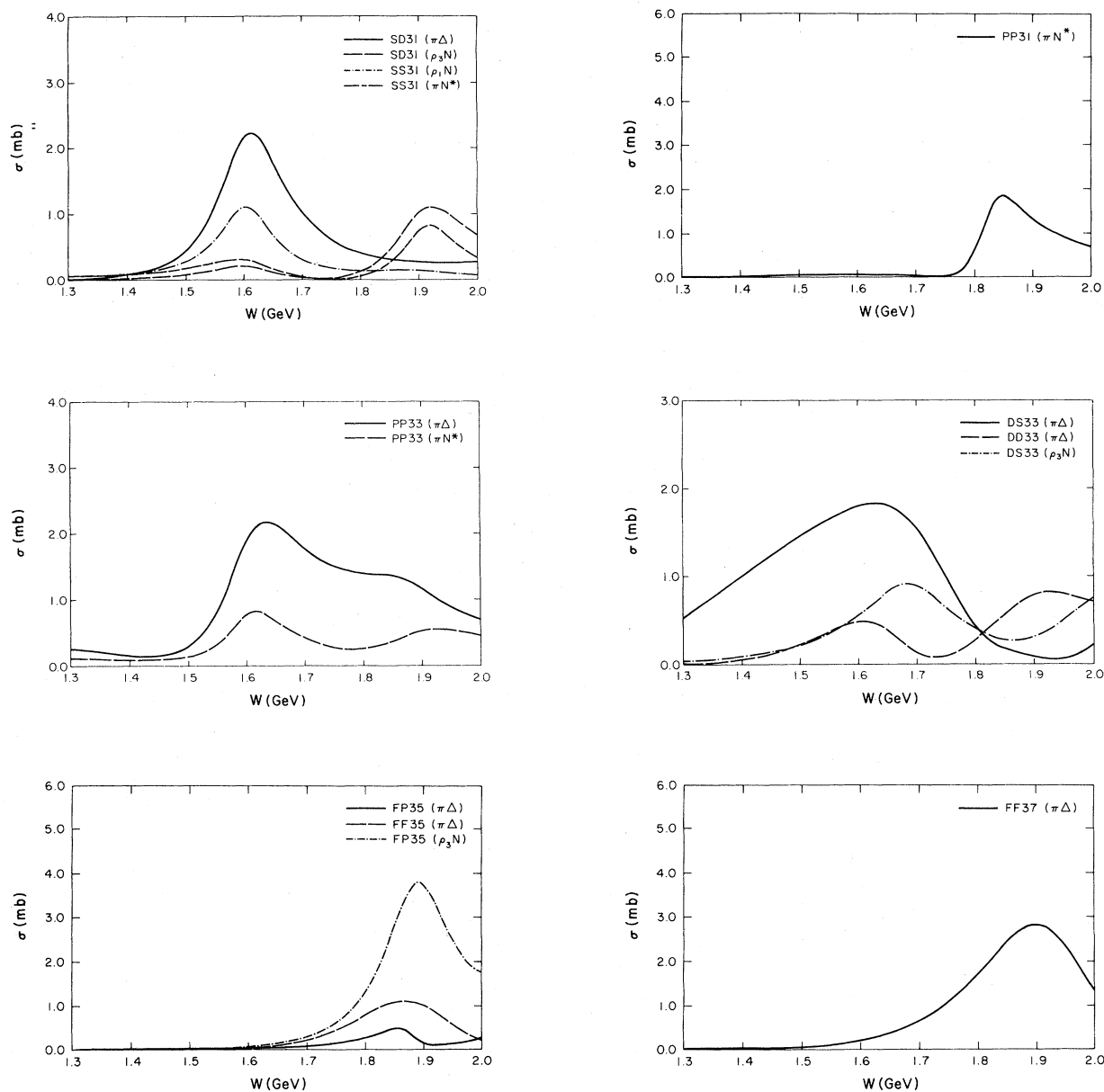
FIG. 4. (Continued.)

D_{35}. We find no evidence for $\pi\pi N$ inelasticity in this wave although EPSA predict a cross section of about 3 mb. In particular, the amplitudes $DP35(\pi D_{13})$ and $DS35(\pi F_{15})$, which the Berkeley-SLAC collaboration had suggested as possibly being important,[1] were searched and found to be negligible. We suggest that the $D_{35}(1930)$ decays dominantly to $\pi\pi\pi N$ via the waves $DS35(\rho\Delta)$ and/or $DP35(\epsilon\Delta)$.

F_{35}. Our analysis accounts for most of the F_{35} inelasticity with ρN the dominant decay channel. In agreement with previous inelastic analyses, we find the f-wave $\pi\Delta$ decay amplitude to be larger than the p-wave amplitude.

F_{37}. Our analysis accounts for about a third of the F_{37} inelasticity with $\pi\Delta$ the dominant $\pi\pi N$ decay channel of the $F_{37}(1950)$ resonance. Our study of πN^* decay channels indicates that this resonance also has a significant $\pi N^*(F_{15})$ decay. Most of the unobserved inelasticity may be due to decay of the $F_{37}(1950)$ into $\pi\pi\pi N$ via the wave $FP37(\rho\Delta)$.

G_{37}. We see no evidence of $\pi\pi N$ inelasticity in this wave.

B. Reaction cross sections

Our fitted reaction cross sections are presented in Table VII and Fig. 5. Figure 5 also compares our fitted values with the experimental measurements[9-11,23] by means of a curve fitted to link the results of our energy-independent
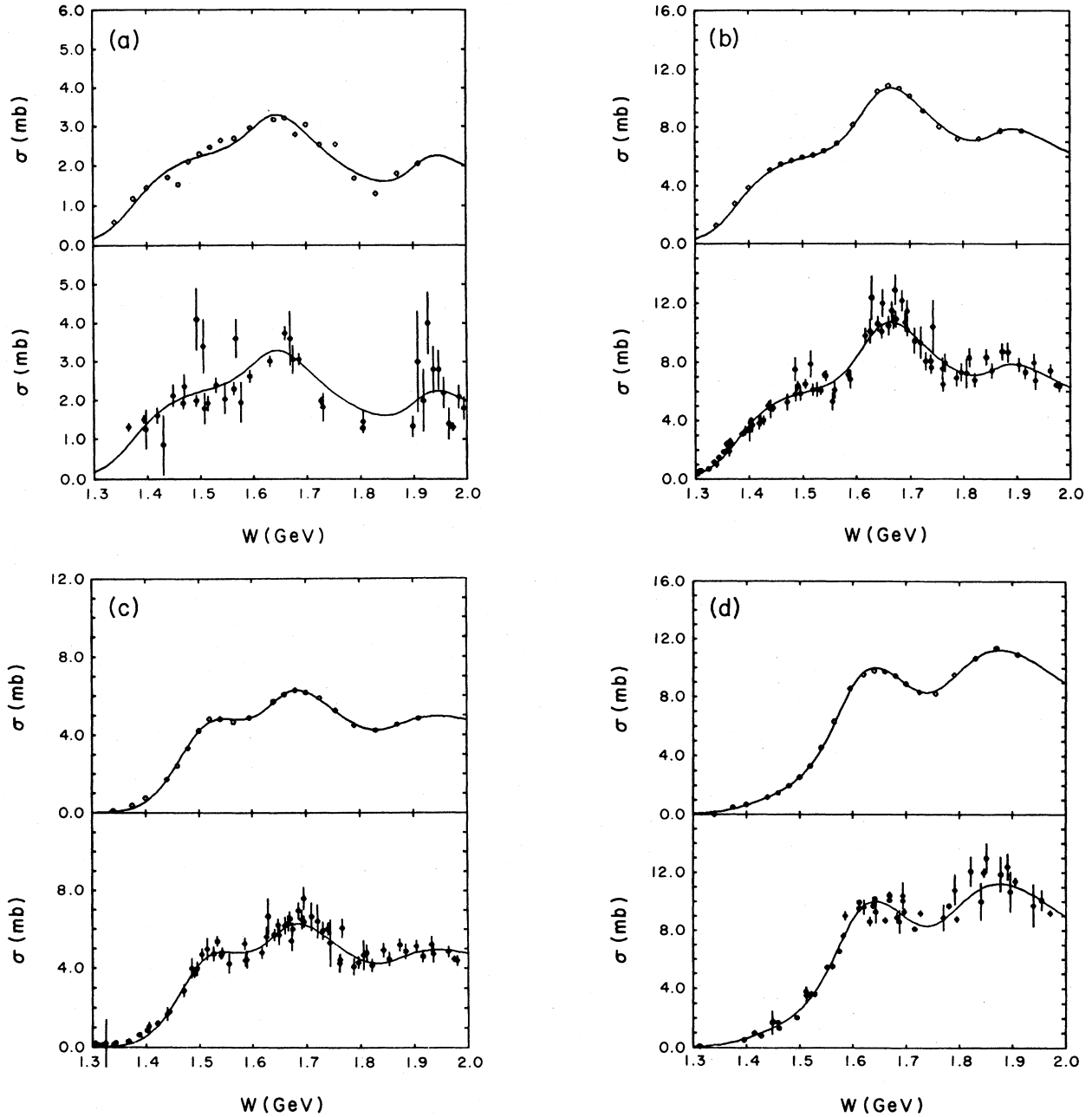
FIG. 5. Reaction cross sections for (a) $\pi^- p \to \pi^0 \pi^0 n$, (b) $\pi^- p \to \pi^+ \pi^- n$, (c) $\pi^- p \to \pi^0 \pi^- p$, (d) $\pi^+ p \to \pi^0 \pi^+ p$, and (e) $\pi^+ p \to \pi^+ \pi^+ n$. Results of our energy-independent analysis are presented in the upper parts with experimental values in the lower parts. The reaction $\pi^- p \to \pi^0 \pi^0 n$ was predicted at all energies by fitting data for the other four charge channels. The curves were obtained from energy-dependent fits of our results for each charge channel.

fits. The reaction $\pi^- p \to \pi^0 \pi^0 n$ is predicted at all energies and agrees very well with the rather poorly determined experimental measurements. At some energies (see Table I), where data were unavailable, we also predicted cross sections for the reactions $\pi^+ p \to \pi^0 \pi^+ p$ and $\pi^+ p \to \pi^+ \pi^+ n$. Our fitted cross sections are generally in excellent agreement with the measured ones except for $\pi^+ p \to \pi^+ \pi^+ n$ above 1700 MeV where our cross sections are about 1 mb smaller than the measured ones. Nevertheless, in view of the large experimental errors, our results are not too inconsistent with these measurements.

C. Determination of overall phase

As with any analysis of this sort, the overall phase of the amplitudes at each energy must be determined by performing a multichannel K-matrix analysis, by assuming a specific energy dependence (e.g., Breit Wigner) for one or
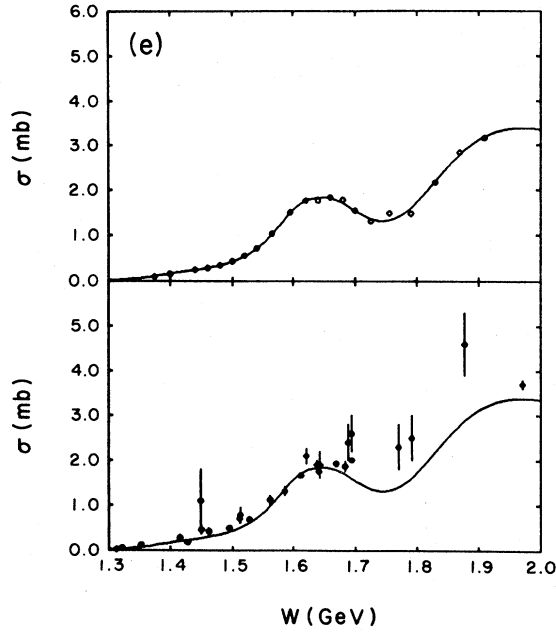
FIG. 5. (*Continued.*)

more amplitudes, or by performing some kind of "minimum-path" analysis. For the present analysis, we have utilized a combination of the last two techniques. In the vicinity of a single strong resonance and in the absence of a large background, the elastic and inelastic amplitudes should share a common phase (modulo π). We assumed that these conditions were satisfied for the

TABLE VII. Reaction cross sections (in mb) determined from this analysis.

W (MeV)	$\pi^0\pi^0 n$	$\pi^+\pi^- n$	$\pi^0\pi^- p$	$\pi^0\pi^+ p$	$\pi^+\pi^+ n$
1340	0.59	1.27	0.12	0.01	0.00
1375	1.18	2.77	0.39	0.52	0.10
1400	1.45	3.87	0.76	0.70	0.16
1440	1.71	5.09	1.72	1.20	0.25
1460	1.53	5.49	2.43	1.48	0.29
1480	2.10	5.74	3.33	1.99	0.35
1500	2.29	5.96	4.22	2.57	0.44
1520	2.47	6.10	4.83	3.32	0.56
1540	2.64	6.39	4.82	4.54	0.72
1565	2.69	6.92	4.67	6.33	1.04
1595	2.96	8.17	4.88	8.57	1.51
1620				9.55	1.77
1640	3.17	10.47	5.71	9.81	1.77
1660	3.21	10.86	6.07	9.76	1.84
1680	2.79	10.68	6.28	9.47	1.79
1700	3.04	10.16	6.17	8.91	1.55
1725	2.53	9.12	5.89	8.34	1.31
1755	2.54	8.04	5.25	8.24	1.49
1790	1.68	7.21	4.50	9.54	1.48
1830	1.30	7.20	4.24	10.67	2.17
1870	1.80	7.74	4.54	11.39	2.84
1910	2.05	7.76	4.84	10.95	3.16

$D_{13}(1520)$, $D_{15}(1675)$, and $F_{37}(1950)$ resonances. For an initial determination of the overall phase at each energy, we assumed the phase of $DS\,13(\rho_3 N)$ to be the same as the elastic D_{13} amplitude in the energy range 1320 to 1580 MeV, we assumed the phase of $DD\,15(\pi\Delta)$ to be the same as the elastic D_{15} amplitude in the energy range 1580 to 1740 MeV, and we assumed the phase of $FF\,37(\pi\Delta)$ to be the same as the elastic F_{37} amplitude in the energy range 1740 to 1930 MeV. The phases that result from this procedure are reasonably continuous over the boundaries at 1580 and 1740 MeV. Near threshold, the inelastic D_{13} phases are nearly real as required by unitarity. The overall phase above 1740 MeV could have been determined using the F_{35} partial wave which has an observed resonance at 1905 MeV. Quark models, however, predict two F_{35} resonances above 1900 MeV (Ref. 6) and, therefore, the assumption of a single resonance is probably invalid. This problem does not arise for the F_{37} wave since the observed F_{37} resonance is the only one predicted to lie in this energy range. Further support for our choice is given by the $GD17(\rho_3 N)$ wave which we find to be nearly real, as expected for the just opening G_{17} channel.

After obtaining initial estimates for the overall phase at each energy, we performed a constrained minimum-path analysis by minimizing the quantity

$$\chi^2_{\text{path}} = \sum_{i,j} |\Delta A_{i,j}|^2 / \Delta W_j^2$$
$$+ \sum_j (\Phi_j - \phi_j)^2 / \Delta\phi_j^2 , \qquad (6.1)$$

where $|\Delta A_{i,j}|^2$ is the absolute square of the difference in the ith partial-wave amplitude at the jth and $(j+1)$th energies, ΔW_j is the difference in the jth and $(j+1)$th energies, ϕ_j is a constrained rotation phase determined from comparison with resonant elastic waves, $\Delta\phi_j$ is the assigned error (± 0.3 radians) in ϕ_j, and Φ_j is the searched rotation phase. We weighted $|\Delta A_{i,j}|^2$ by the errors in the associated partial-wave amplitudes and only included contributions from amplitudes with moduli greater than 0.05. Only about half of the phases searched were constrained by terms in the second sum.

E. Phase conventions

For convenience in comparing our results with those of other analyses and with predictions of various theoretical models, we adjusted our amplitudes to comply with the now standard "baryon-first" phase convention. In this convention, the baryon always appears before the meson in all isospin Clebsch-Gordan coefficients (CGC's). Furthermore, spin couplings in all angular momentum CGC's are ordered such that orbital angular momentum L comes before intrinsic spin S. Finally, the angles in the $Y_{l,m}$'s are always measured with respect to the first particle in the corresponding isospin CGC's. The (present) amplitudes which derive from the formalism presented in Sec. III are related to those of the standard convention as follows:

$$A_\epsilon(\text{standard}) = A_\epsilon(\text{present}) , \qquad (6.2a)$$

$$A_{\rho_1}(\text{standard}) = A_{\rho_1}(\text{present}) , \qquad (6.2b)$$

$$A_{\rho_3}(\text{standard}) = -A_{\rho_3}(\text{present}) , \qquad (6.2c)$$

$$A_{\Delta}(\text{standard}) = (-)^{l_I + I + 1/2} A_{\Delta}(\text{present}) , \qquad (6.2d)$$

$$A_N^*(\text{standard}) = (-)^{l_I + I - 1/2} A_N^*(\text{present}) . \qquad (6.2e)$$

The results of this analysis, including numerical values of the partial-wave amplitudes, are available through an interactive computing facility at VPI&SU called "SAID" for "scattering analyses interactive dial-in." A recent description of SAID can be found in Ref. 29.

F. Partial-wave amplitudes

In this paper, we shall refrain from a detailed resonance analysis of our partial-wave amplitudes and instead only comment upon the magnitudes of amplitudes at resonance and their signs, when apparent. Argand diagrams are plotted for each amplitude in Fig. 6 in accordance with

the baryon-first phase convention. The results of our energy-independent fits for the real and imaginary parts of each amplitude are also shown. The curves in Figs. 4 and 6 were obtained from energy-dependent fits to the complex amplitudes. We caution the reader against taking the fitted curves too seriously at energies where the energy-independent amplitudes were either noisy or unmeasured (e.g., between 1900 and 2000 MeV). In the discussion which follows, we shall discuss couplings to both established and proposed resonances. We denote resonances by their $SU(6) \times O(3)$ classification $(D, L^P)_N$, where D is the dimensionality of the supermultiplet, L is the total orbital angular momentum, P is the parity, and N is the number of quanta of excitation characterizing a given band of multiplets. On occasion, we will suffix the resonance assignment by $(SU(3), SU(2))$, where $SU(3)$ and $SU(2)$ denote the $SU(6)$ subgroup content of the state.

$S_{11}(1535)$. This $(70, 1^-)_1$ resonance is observed coupling so $SP11(\epsilon N)$ and $SS11(\rho_1 N)$. Both amplitudes are
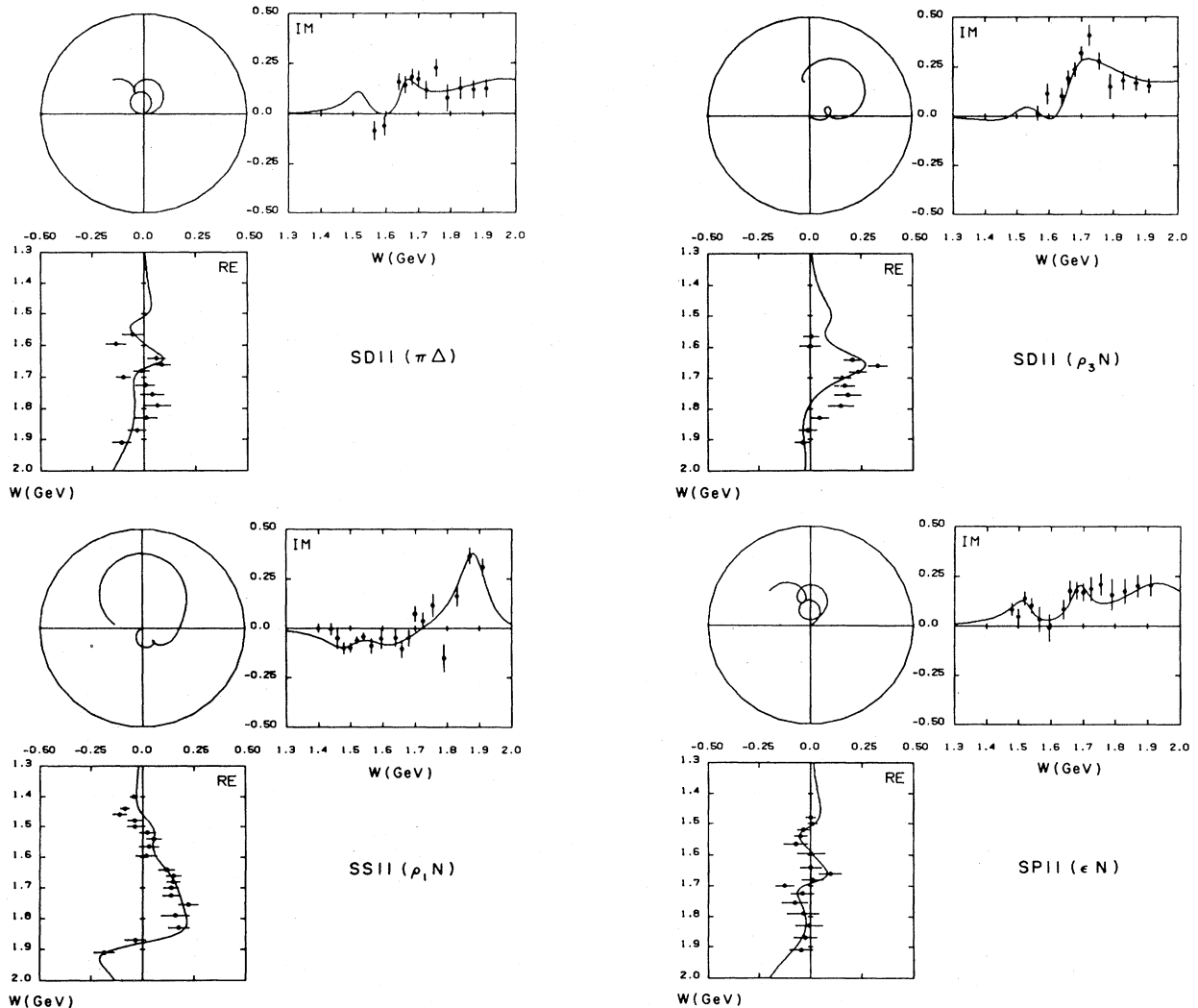

FIG. 6. Argand diagrams for the quasi-two-body amplitudes. The results of our energy-independent analysis are shown in the projections of the real and imaginary parts. Displayed errors are twice as large as those obtained from our fitting algorithm. The curves were obtained from energy-dependent fits of the amplitudes.
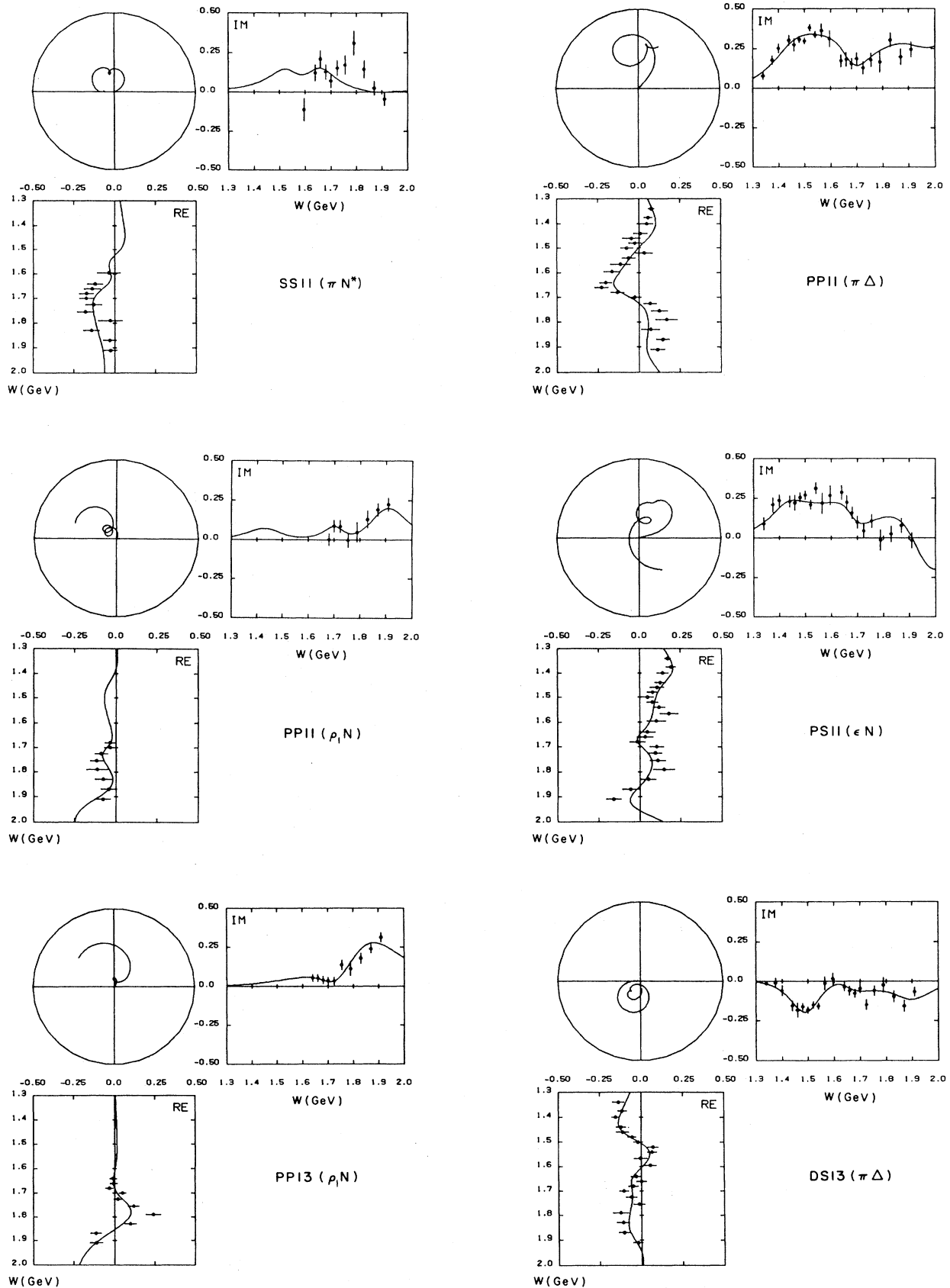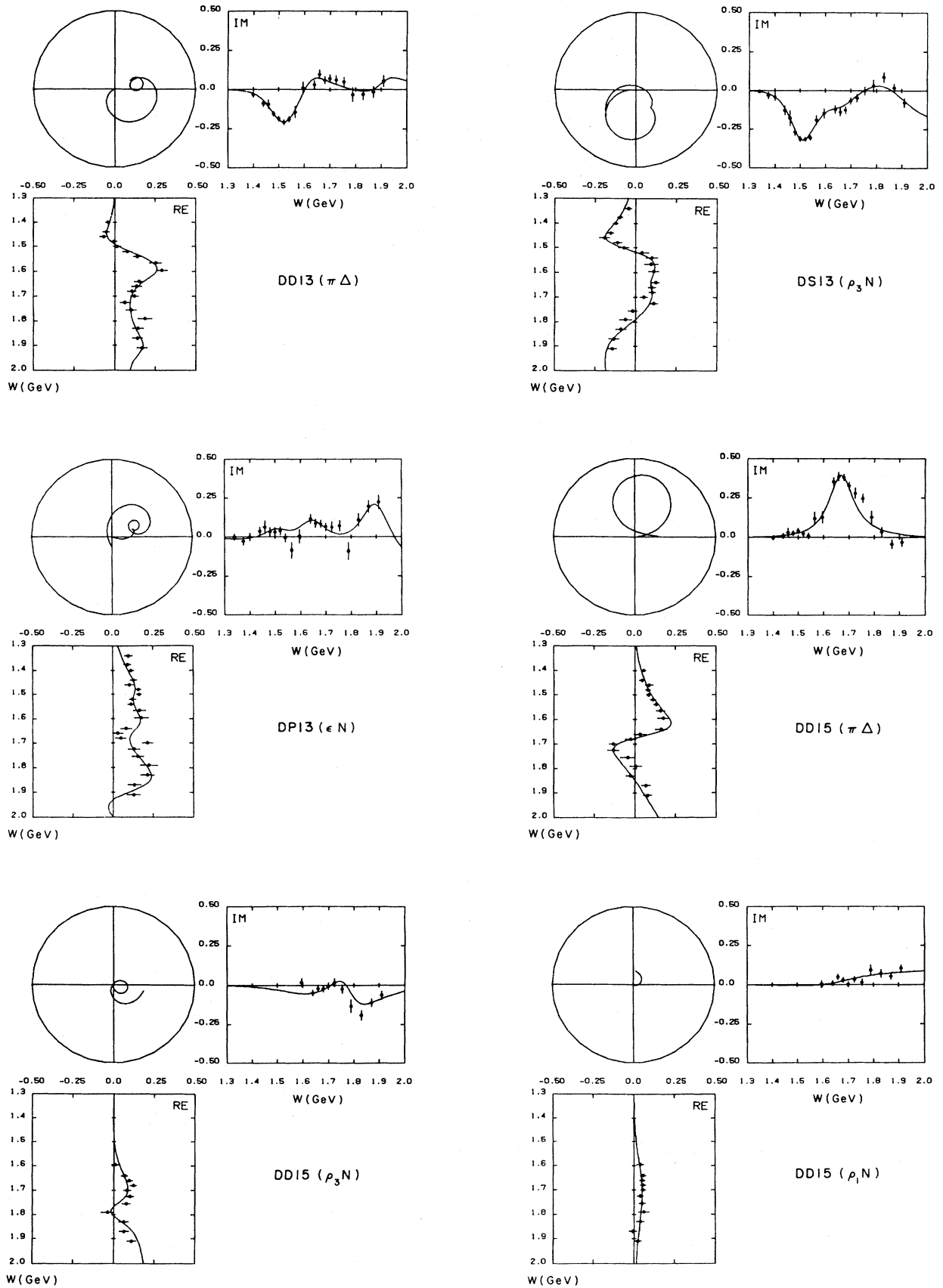
FIG. 6. (Continued.)

DD13 ($\pi\Delta$)

DS13 ($\rho_3 N$)

DP13 (ϵN)

DD15 ($\pi\Delta$)

DD15 ($\rho_3 N$)

DD15 ($\rho_1 N$)

FIG. 6. (*Continued.*)

FP15 ($\pi \triangle$)

FF15 ($\pi \triangle$)

FP15 ($\rho_3 N$)

FF15 ($\rho_3 N$)

FD15 (ϵN)

GD17 ($\rho_3 N$)

FIG. 6. (Continued.)

SD31 ($\pi\Delta$)

SD31 ($\rho_3 N$)

SS31 ($\rho_1 N$)
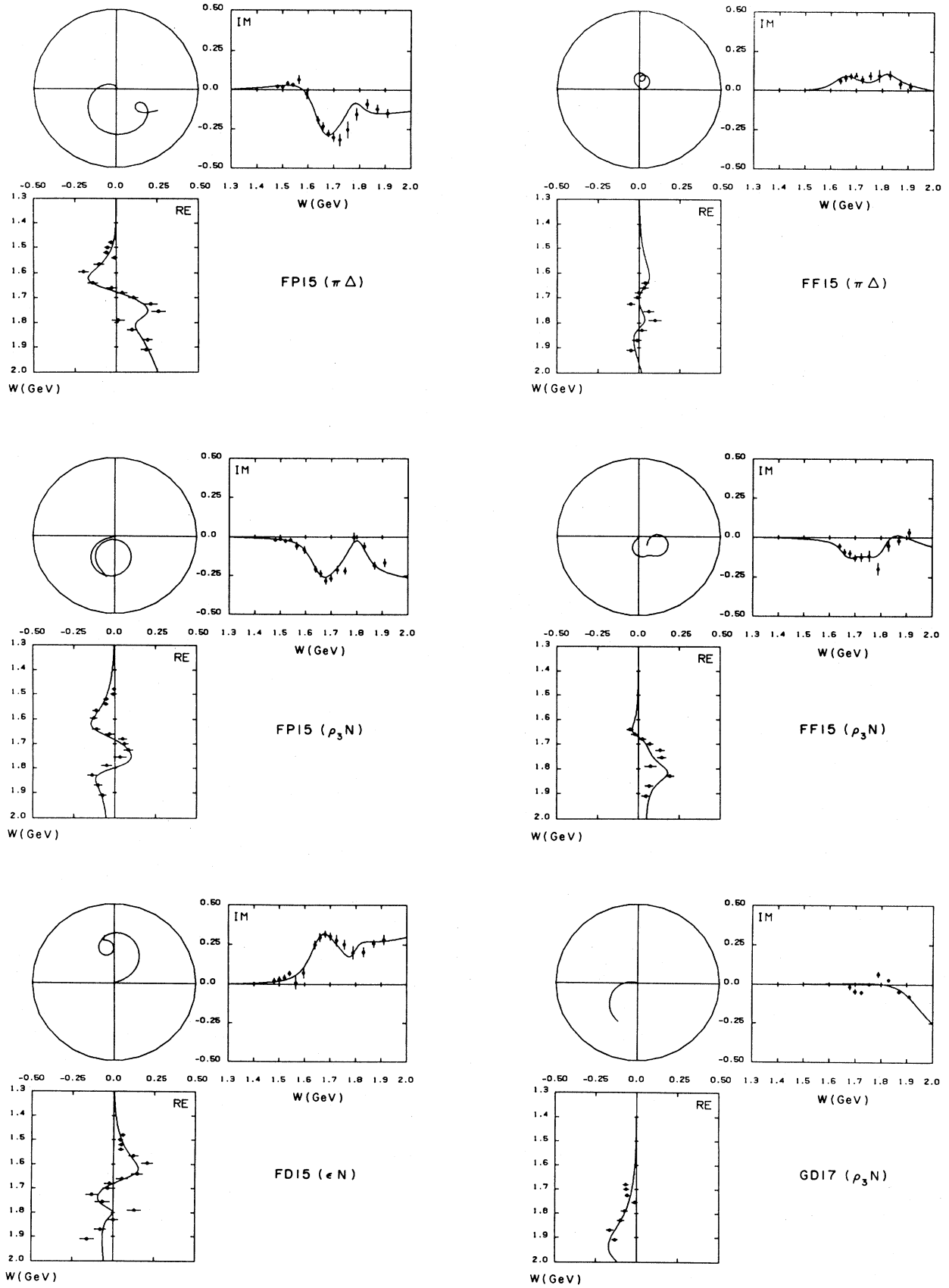
SS31 (πN^*)

PP31 (πN^*)

PP33 ($\pi\Delta$)
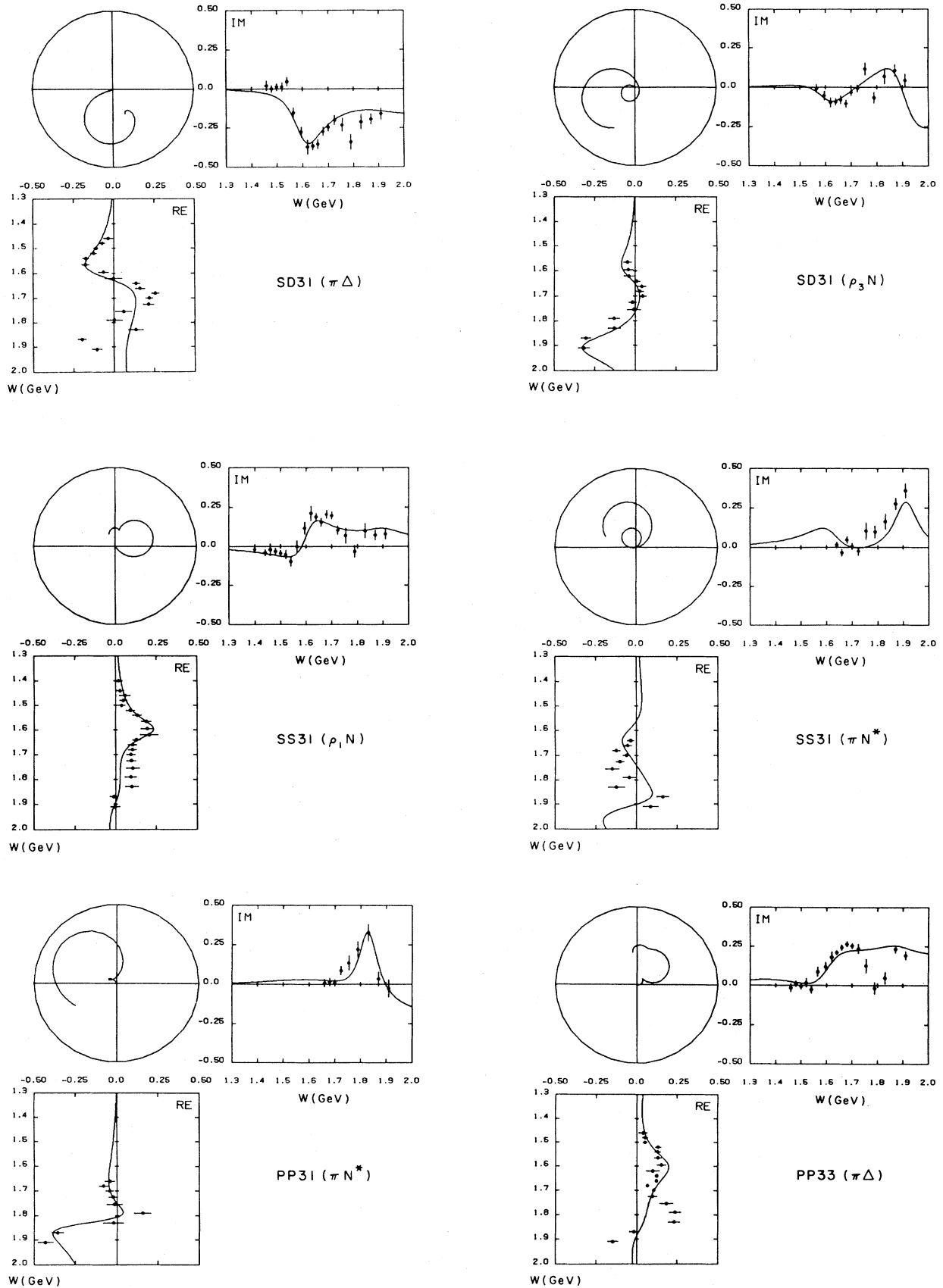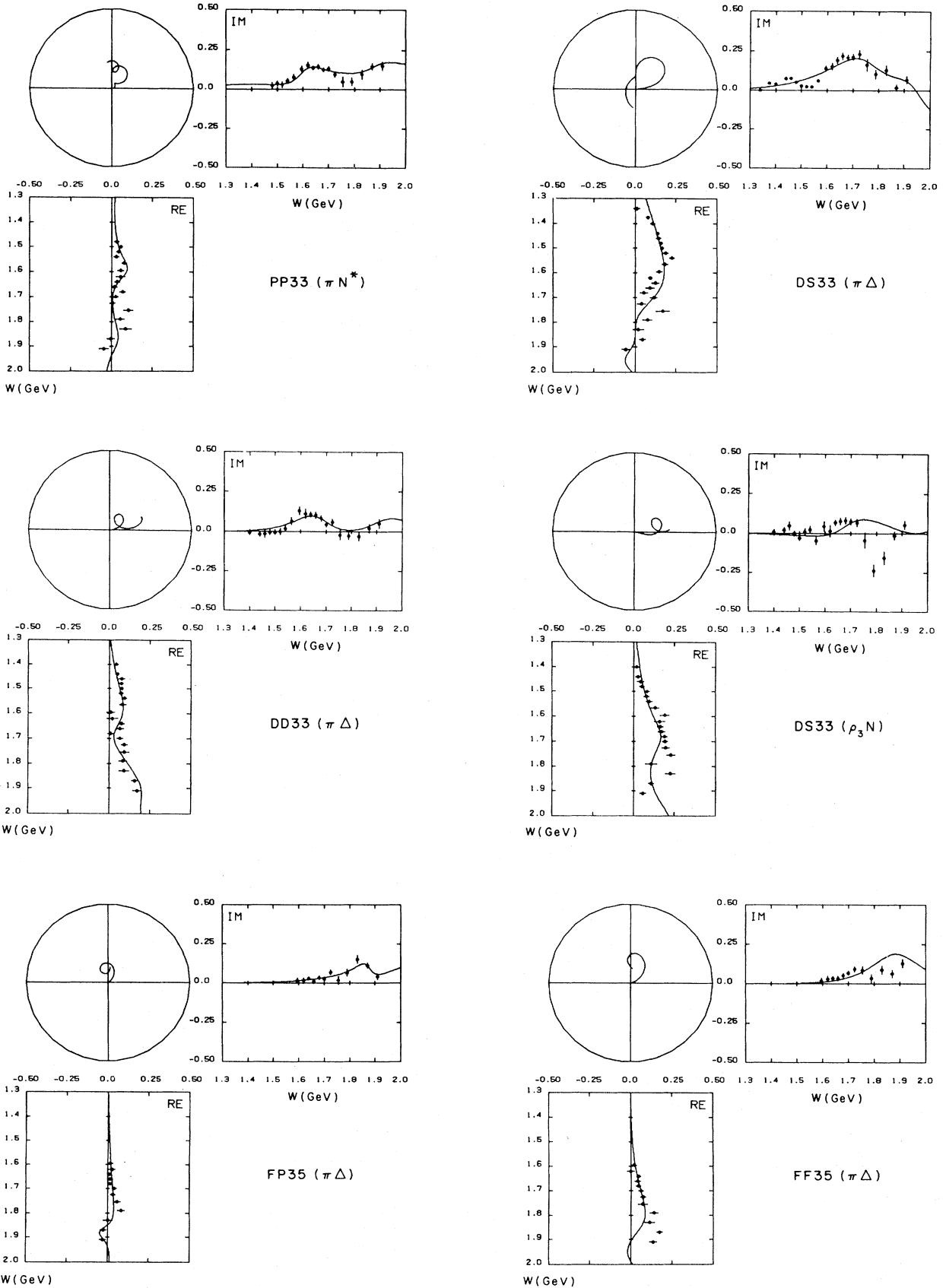
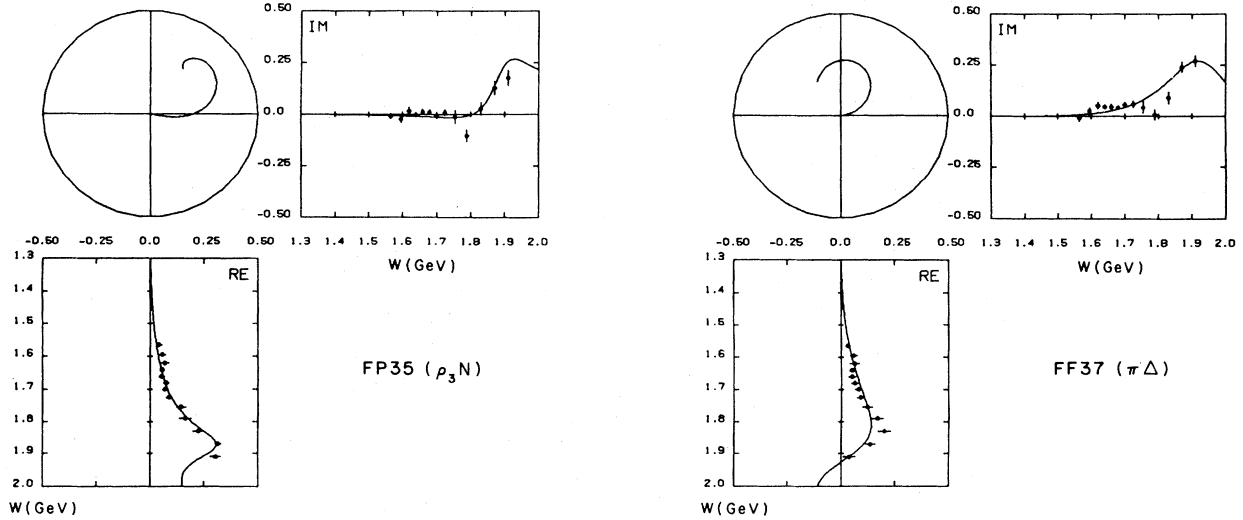FIG. 6. (*Continued.*)

FIG. 6. (Continued.)

FIG. 6. (Continued.)

small with the sign of $SP\,11(\epsilon N)$ positive and the sign of $SS\,11(\rho_1 N)$ negative.

$S_{11}(1650)$. Couplings of this $(70,1^-)_1$ resonance are somewhat uncertain because of its proximity to the $S_{11}(1535)$. We are fairly sure that the sign of $SS\,11(\rho_1 N)$ is negative and that the signs of $SP\,11(\epsilon N)$ and $SS\,11(\pi N^*)$ are positive. Both $SD\,11(\pi\Delta)$ and $SD\,11(\rho_3 N)$ are fairly large. The sign of $SD\,11(\pi\Delta)$ is probably positive whereas the sign of $SD\,11(\rho_3 N)$ is unclear.

$S_{11}(1900)$. We possibly observe a $(56,1^-)_3$ resonance with a mass of about 1900 MeV coupling to $SS\,11(\rho_1 N)$ and $SD\,11(\pi\Delta)$. Their signs are both positive. It probably also couples to $SP\,11(\epsilon N)$ although the sign is unclear.

$P_{11}(1440)$. This $(56,0^+)_2$ resonance is observed coupling to both $PS\,11(\epsilon N)$ and $PP\,11(\pi\Delta)$. Both amplitudes are large with positive signs.

$P_{11}(1710)$. This $(70,0^+)_2$ resonance couples to $PP\,11(\pi\Delta)$ and possibly $PS\,11(\epsilon N)$ and $PP\,11(\rho_1 N)$ as well. The sign of $PP\,11(\pi\Delta)$ is probably negative whereas the sign of $PP\,11(\rho_1 N)$ is probably positive. The sign of $PS\,11(\epsilon N)$ is unclear.

$P_{11}(1900)$. We possibly observe a $(56,2^+)_2$ resonance near 1900 MeV coupling weakly to $PP\,11(\pi\Delta)$, $PS\,11(\epsilon N)$, and $PP\,11(\rho_1 N)$. The signs of $PS\,11(\epsilon N)$ and $PP\,11(\pi\Delta)$ are probably negative, whereas the sign of $PP\,11(\rho_1 N)$ is probably positive.

$P_{13}(1720)$. We do not clearly observe any $\pi\pi N$ channel coupling appreciably to this $(56,2^+)_2$ resonance.

$P_{13}(1850)$. We possibly observe a $(70,0^+)_2$ resonance with a mass of about 1850 MeV that couples to $PP\,11(\rho_1 N)$. The sign of the amplitude is positive.

$D_{13}(1520)$. This $(70,1^-)_1$ resonance clearly has large couplings to $DS13(\pi\Delta)$, $DD\,13(\pi\Delta)$, and $DS13(\rho_3 N)$. The signs of all three amplitudes are negative.

$D_{13}(1700)$. This $(70,1^-)_1$ resonance appears to have small couplings to $DS\,13(\pi\Delta)$, $DD\,13(\pi\Delta)$, and $DP\,13(\epsilon N)$. The signs of $DP\,13(\epsilon N)$ and $DD\,13(\pi\Delta)$ are probably positive, whereas the sign of $DS\,13(\pi\Delta)$ is un-

clear.

$D_{13}(1900)$. There is some evidence for a $(56,1^-)_3$ resonance with significant couplings to $DP\,13(\epsilon N)$ and $DS13(\rho_3 N)$. There may also be a weak coupling to $DS\,13(\pi\Delta)$. The signs of $DP\,13(\epsilon N)$ and $DS\,13(\rho_3 N)$ are probably positive whereas the sign of $DS\,13(\pi\Delta)$ is probably negative.

$D_{15}(1675)$. This $(70,1^-)_1$ resonance is clearly observed with a large coupling to $DD\,15(\pi\Delta)$. There is also a small coupling to $DD15(\rho_3 N)$. The sign of $DD\,15(\pi\Delta)$ is positive and the sign of $DD\,15(\rho_3 N)$ is probably negative.

$F_{15}(1680)$. This $(56,2^+)_2$ resonance has large couplings to $FP\,15(\pi\Delta)$, $FP\,15(\rho_3 N)$, and $FD\,15(\epsilon N)$ and smaller couplings to $FF\,15(\pi\Delta)$ and $FF\,15(\rho_3 N)$. We clearly observe the signs of $FP\,15(\pi\Delta)$, $FP\,15(\rho_3 N)$, and $FF\,15(\rho_3 N)$ to be negative and the signs of $FD\,15(\epsilon N)$ and $FF\,15(\pi\Delta)$ to be positive.

$F_{15}(1850)$. We observe a $(70,0^+)_2$ resonance with a mass near 1850 MeV. There is a large coupling to $FP\,15(\rho_3 N)$ with smaller couplings to $FP\,15(\pi\Delta)$, $FF\,15(\pi\Delta)$, $FD\,15(\epsilon N)$, and probably $FF\,15(\rho_3 N)$. The signs of $FP\,15(\rho_3 N)$, $FP\,15(\pi\Delta)$, and $FF\,15(\pi\Delta)$ are probably positive whereas the signs of $FD\,15(\epsilon N)$ and $FF\,15(\rho_3 N)$ are unclear.

$G_{17}(2190)$. We observe the tail of this resonance which has a large coupling to $GD\,17(\rho_3 N)$. The sign of the amplitude is negative.

$S_{31}(1620)$. This $(70,1^-)_1$ resonance is clearly observed with large couplings to $SD31(\pi\Delta)$ and $SS31(\rho_1 N)$. There is also a small coupling to $SD31(\rho_3 N)$. The signs of $SD\,31(\pi\Delta)$ and $SD\,31(\rho_3 N)$ are negative whereas the sign of $SS\,31(\rho_1 N)$ is positive.

$S_{31}(1900)$. We possibly observe a $(56,1^-)_3$ resonance with a mass of about 1900 MeV associated with an observed inelastic S_{31} cross section of about 2 mb. Unfortunately, our S_{31} amplitudes are rather noisy above about 1750 MeV. There are large couplings to $SS\,31(\pi N^*)$ and probably $SD\,31(\rho_3 N)$. The sign of $SS\,31(\pi N^*)$ is probably positive whereas the sign of $SD\,31(\pi\Delta)$ is unclear.

$P_{31}(1910)$. The $PP\,31(\pi N^*)$ wave seems to account for

all of the observed inelasticity in the P_{31} partial wave. Resonance behavior is unclear although there may be coupling to a resonance with mass between 1800 and 1900 MeV. The sign of the amplitude is probably positive.

$P_{33}(1600)$. We observe this $(56,0^+)_2$ resonance to have fairly large couplings to $PP33(\pi\Delta)$ and $PP33(\pi N^*)$. The signs of both amplitudes are positive.

$P_{33}(1920)$. We probably observe a $(56,2^+)_2$ resonance with a mass near 1900 MeV coupling to $PP33(\pi\Delta)$ and $PP33(\pi N^*)$. The signs of both amplitudes are probably positive.

$D_{33}(1700)$. This $(70,1^-)_1$ resonance is observed coupling to $DS33(\pi\Delta)$, $DD33(\pi\Delta)$, and $DS33(\rho_3N)$. The signs of all three amplitudes are probably positive. Above 1700 MeV, none of the amplitudes exhibit characteristic resonance behavior, possibly because of interference from a higher mass D_{33} resonance.

$F_{35}(1905)$. The Isgur-Karl quark model predicts a $(56,2^+)_2$ resonance at 1940 MeV and a $(70,2^+)_2$ resonance at 1975 MeV.[6] We observe evidence for one or more F_{35} resonances above 1900 MeV coupling to $FP35(\pi\Delta)$, $FF35(\pi\Delta)$, and $FP35(\rho_3N)$. The signs of all three amplitudes are positive.

$F_{37}(1950)$. This $(56,2^+)_2$ resonance is observed with a large coupling to $FF37(\pi\Delta)$. The sign of the amplitude is clearly positive.

VII. COMPARISONS WITH OTHER WORKS

In the first part of this section, we discuss previous major partial-wave analyses of $\pi N \to \pi\pi N$. We first compare general features such as energy range of the analysis, assumptions regarding quasi-two-body channels, the amount of data fitted, the fitting technique, and amplitude parametrizations. The next three parts compare the present solution with those of the Berkeley-SLAC,[1] Saclay,[2] and Imperial College[3] analyses. Next, we discuss several theoretical models to predict various resonance couplings. Finally, we compare the signs of resonant amplitudes determined unambiguously from the major experimental analyses with theoretical predictions.

A. Previous analyses

An early investigation of $\pi N \to \pi\Delta$ amplitudes was carried out in 1971 by a Berkeley-SLAC collaboration.[30] This group performed an energy-dependent partial-wave analysis of the reaction $\pi^- p \to \pi^+ \Delta^-$ at 11 energies in the c.m. energy range 1640 to 1760 MeV. Their data were obtained from 20 248 $\pi^- p \to \pi^+ \pi^- n$ events. In a later work discussed below, their study was extended to a detailed isobar-model partial-wave analysis of $\pi N \to \pi\pi N$ between 1300 and 2000 MeV.[1]

Early information about $\pi N \to \pi\Delta$ amplitudes was also obtained from an energy-dependent partial-wave analysis of the reaction $\pi^+ p \to \pi^0 \Delta^{++}$ performed in 1972 by a Berkeley-Riverside collaboration.[9] Their data were obtained from 35 400 $\pi^+ p \to \pi^0 \pi^+ p$ events at six energies in the c.m. energy range 1820 to 2090 MeV. This group first discovered the curious dominance of f- over p-wave $\pi\Delta$ decay of the $F_{35}(1905)$ resonance. They also found that the $D_{35}(1930)$ and $P_{31}(1910)$ resonances had negligible

couplings to the $\pi\Delta$ channel. Their findings are corroborated by the present analysis as well as by the Berkeley-SLAC analysis[1] discussed below.

In 1974, the Berkeley-SLAC collaboration completed an energy-independent, isobar-model analysis of $\pi N \to \pi\pi N$ at 18 energies between 1300 and 2000 MeV.[1] At that time, however, no data were available for fitting between 1540 and 1640 MeV. A total of 163 297 events from the channels $\pi^- p \to \pi^+ \pi^- n$, $\pi^- p \to \pi^0 \pi^- p$, and $\pi^+ p \to \pi^0 \pi^+ p$ were fitted by the maximum-likelihood technique assuming quasi-two-body channels $\pi\Delta$, ρN, and ϵN. Two continuous solutions, A and B, were found that were similar in regions with data but had different continuations through the energy gap. Solution A was later discarded in favor of solution B when data in the gap later became available for fitting.[31] Our comparisons below with the Berkeley-SLAC analysis shall refer strictly to solution B.

Early isobar-model analyses performed at Saclay were restricted to either $\pi^+ p$ or $\pi^- p$ reactions and were limited in the number of waves used.[32] A more extensive analysis was completed at Saclay in 1976 in which 91 314 events from the channels $\pi^- p \to \pi^+ \pi^- n$, $\pi^- p \to \pi^0 \pi^- p$, and $\pi^+ p \to \pi^0 \pi^+ p$ were fitted assuming production of $\pi\Delta$, ρN, and ϵN.[2] The analysis was performed at nine energies between 1360 and 1760 MeV. Data were fitted by the method of least χ^2 after events at each energy had been binned in Dalitz-plot zones of constant πN effective mass.

In 1977, Novoseller investigated the stability of the Berkeley-SLAC solution under the perturbation of including a one-pion-exchange (OPE) background contribution for high partial waves.[27] He concluded that the $I_{\pi\pi} = 2$ contribution was small below 1970 MeV and could probably be ignored. He also found that the $GD17(\rho_3N)$ amplitude contributed over half of the total OPE high-partial-wave cross section. This wave was included among those searched in the present analysis and was found to be the only significant wave with $l=4$. Novoseller's analysis raised doubts about some features of the Berkeley-SLAC solution. For example, he found that the F_{35} partial-wave cross section above 1750 MeV was unstable to both partial-wave constraints (used by Berkeley-SLAC) and to inclusion of a OPE background. Thus, Berkeley-SLAC's procedure of using both the $F_{35}(1905)$ and $F_{37}(1950)$ resonance to determine the overall phase of their solution above 1730 MeV is questionable. We share Novoseller's doubts concerning the F_{35} wave for reasons discussed in the previous section. Novoseller's analysis also raised doubts about the large coupling in the Berkeley-SLAC solution of the $P_{13}(1720)$ resonance to $PP13(\rho_1N)$. His results, like those of the present analysis, are instead consistent with a P_{13} resonance somewhat above 1800 MeV.

In 1979, Arndt et al.[12] investigated the reaction $\pi^- p \to \pi^+ \pi^- n$ below 1400 MeV by fitting 4140 bubble-chamber events. Data were fitted using an isobar model which incorporated a background calculated from a generalized phenomenological πN Lagrangian. In this energy range, the reaction is dominated by the tail of the Roper resonance, with ϵN the dominant intermediate state. The $PP11(\pi\Delta)$, $PS11(\epsilon N)$, $DS13(\pi\Delta)$, and $DS33(\pi\Delta)$ ampli-

tudes fitted in this analysis agree approximately in both magnitude and phase with the results of the present analysis. The searched phase of $PS11(\epsilon N)$ was about 30° greater in the earlier analysis, however, which is consistent with a small, positive part of the amplitude coming from the background term.

Another isobar-model analysis was completed fairly recently at Imperial College.[3] The Imperial College group used a maximum-likelihood technique to fit 43 589 events from the channels $\pi^+p\rightarrow\pi^0\pi^+p$ and $\pi^+p\rightarrow\pi^+\pi^+n$ assuming production of $\pi\Delta$, ρN, and $\pi N^*(P_{11})$. Hence, only $I=\frac{3}{2}$ amplitudes were determined by their analysis. This group was the first to systematically search $\pi N\rightarrow\pi N^*$ amplitudes and to fit data from the $\pi^+p\rightarrow\pi^+\pi^+n$ channel. Their analysis was carried out at nine energies between 1400 and 1700 MeV and included a OPE contribution from s-wave $\pi\pi$ scattering in the $I_{\pi\pi}=2$ channel. Solutions with the OPE contribution were similar to those without it. They found a nearly constant OPE cross section of about 0.3 mb whereas the total $I=\frac{3}{2}$ cross section increases from about 1 to 12 mb in the same energy range. The Imperial College group felt that the OPE contribution was significant, however, since they obtained consistent values of the s-wave isotensor $\pi\pi$ scattering length at different energies.

It is worthwhile to compare two more distinguishing features of these various analyses. Neither the present analysis nor that of the Imperial College group imposed partial-wave constraints to satisfy unitarity limits as did both the Berkeley-SLAC and Saclay groups. Thus, the former two analyses are independent of elastic phase-shift analyses whereas the latter two are not. In regard to the parametrization of barrier-penetration factors, both the Berkeley-SLAC and Imperial College groups used the low-momentum form, p^l, whereas the form used by Saclay $[x/(1+x^2)^{1/2}]^l$ with $x=pR$ and $R=\frac{1}{4}$ fm, was more similar to the Blatt-Weisskopf form (cf. Table II) of the present work.

B. Comparison with the Berkeley-SLAC solution

The most extensive previous analysis was performed by the Berkeley-SLAC collaboration.[1] Their 28-wave solution contains three amplitudes, $PP31(\pi\Delta)$, $PP31(\rho_1N)$, and $FF37(\rho_3N)$, that our procedure found to be small. Both $PP31(\pi\Delta)$ and $PP31(\rho_1N)$ are small waves in the Berkeley-SLAC solution and they account for very little of the P_{31} inelasticity predicted by EPSA. Although $FF37(\rho_3N)$ contributes appreciably to the Berkeley-SLAC solution, several authors have questioned the reliability of its measurement.[5,33] Our final set of waves includes six amplitudes eliminated from the Berkeley-SLAC solution: $SD11(\rho_3N)$, $DD15(\rho_3N)$, $DD15(\rho_1N)$, $FF15(\rho_3N)$, $SD31(\rho_3N)$, and $FP35(\rho_3N)$. Two of these waves, $SD11(\rho_3N)$ and $FF15(\rho_3N)$, contribute appreciably in both the present solution as well as in the Saclay solution,[2] discussed below. Perhaps the most striking difference between the present and Berkeley-SLAC solutions is in the overall phase of amplitudes above 1700 MeV. Near 1900 MeV, for example, the $FF37(\pi\Delta)$ amplitudes of the two solutions differ in phase by about 60°. This phase differ-

ence arises from Berkeley-SLAC's procedure of using the F_{35} resonance to help determine the overall phase above 1730 MeV. As discussed earlier, their procedure possibly suffers from the consequences of two nearby F_{35} resonances. After taking the difference in overall phase into consideration, both analyses are in qualitative agreement for most amplitudes. Several differences occur, however, for low spin waves ($J\leq\frac{3}{2}$). $PP33(\pi\Delta)$ remains a large amplitude in our solution above 1800 MeV, whereas it becomes negligible in the Berkeley-SLAC solution. The opposite effect occurs for $DS33(\rho_3N)$ near 1900 MeV. In the Berkeley-SLAC solution, $PS11(\epsilon N)$ remains a large wave above 1700 MeV, whereas it becomes small in the present solution. Near the $P_{11}(1710)$ resonance, the Berkeley-SLAC solution has a large contribution from $PP11(\rho_1N)$. In the same energy range, our solution has a negligible contribution from this wave.

C. Comparison with the Saclay solution

The Saclay analysis[2] devoted much effort to finding important waves that had been wrongly eliminated from the Berkeley-SLAC solution. In the Saclay solution, only 17 waves were eliminated from the 60 $\pi\Delta$, ρN, and ϵN waves with $J\leq\frac{7}{2}$, $l_i\leq3$, and $l_f\leq3$. When one considers that the F_{35} and F_{37} resonances were beyond the energy range of the Saclay analysis, few waves indeed were eliminated. As a consequence, the 43-wave Saclay solution contains several amplitudes that are small over the energy range of their analysis. Several ρ_3N amplitudes ($SD11$, $PP11$, $DD15$, $FF15$, and $PP31$) eliminated from the Berkeley-SLAC solution contribute appreciably to the Saclay solution. As mentioned above, the present work corroborates Saclay's claims regarding the importance of $SD11(\rho_3N)$ and $FF15(\rho_3N)$. Although the present analysis includes $DD15(\rho_3N)$ as a rather weak effect, we agree with the Berkeley-SLAC result that $PP11(\rho_3N)$ and $PP31(\rho_3N)$ are negligible waves. From K-matrix fits of their amplitudes,[34] the Saclay group identified two low-mass resonances, $P_{13}(1540)$ and $P_{31}(1550)$, as belonging to the $(70,0^+)_2$ multiplet. The present analysis does not detect resonance behavior at such low energies in either the P_{13} or P_{31} waves.

D. Comparison with the Imperial College solution

Since the Imperial College group did not analyze π^-p data, their analysis determined only $I=\frac{3}{2}$ amplitudes.[3] Unlike the Berkeley-SLAC, Saclay, and present analyses, small waves were not eliminated from the Imperial College solution. Their aim in keeping small waves was to minimize the chance of discarding an important wave. Their solution contained a total of 34 amplitudes although, at a given energy, waves above a certain J_{max} were not searched.

The Imperial College analysis found a substantial $\pi N^*(P_{11})$ decay for the P_{33} resonance near 1700 MeV, which the present analysis corroborates. The waves $DD33(\rho_3N)$ and $DD33(\rho_1N)$ contribute appreciably to the Imperial College solution in disagreement with the Berkeley-SLAC, Saclay, and present works. On the other

hand, both Imperial College and Saclay found $DS\,33(\rho_3 N)$ to be a fairly small wave, unlike the Berkeley-SLAC and present analyses. The Imperial College analysis qualitatively agrees with the other analyses discussed above for the large $I = \frac{3}{2}$ waves such as $SD\,31(\pi\Delta)$, $PP\,33(\pi\Delta)$, and $DS\,33(\pi\Delta)$.

E. Models for baryon decay

The current concept of baryons as bound states of three quarks has led to several models for describing their decays by meson emission. If we consider baryons with zero charm, then the underlying internal symmetry group is SU(3) and the symmetry group that includes spin is SU(6). The SU(6) which contains ordinary spin as an SU(2) subgroup forbids various decays known to occur in nature, such as $\Delta \rightarrow \pi N$. These decays are allowed, however, for the group SU(6)$_W$ which contains W-spin as an SU(2) subgroup.[35] Within SU(6)$_W$, hadrons with total internal quark angular momentum L decay to ones with $L = 0$ from an initial state with $L_z = 0$. This situation implies that the internal quarks have momentum only in the z direction. The $\Delta L_z = 0$ nature of SU(6)$_W$ serves to relate amplitudes for decays that differ only by the final orbital angular momentum l_f. In an extended version known as "l-broken SU(6)$_W$," internal quarks are allowed to have transverse momentum.[4] Consequently, $\Delta L_z = \pm 1$ transitions are allowed and amplitudes with different l_f are independent. The l-broken version of SU(6)$_W$ has received theoretical support from work[36] based on the Melosh transformation between current and constituent quarks[37] and PCAC (partially conserved axial-vector current). Since the π and ρ are in the same SU(6)$_W$ multiplet, experimental $\pi N \rightarrow \pi\Delta$ and $\pi N \rightarrow \rho N$ amplitudes can be used to test the validity of SU(6)$_W$ in both its unbroken and l-broken versions. As customary, we refer to phases corresponding to the $\Delta L_z = 0$ condition as having "SU(6)$_W$-like" signs and those corresponding to $\Delta L_z = \pm 1$ as having "anti-SU(6)$_W$" signs.

Various dynamical models based on the SU(6)$\times$O(3) classification of hadrons have been proposed which have more predictive ability than algebraic schemes such as l-broken SU(6)$_W$. One of the more powerful and successful such models is the "naive" quark-pair-creation model (QPCM).[5] In this model, a hadron is assumed to decay by creation of a $q\bar{q}$ pair with the quantum numbers of the vacuum, $J^{PC} = 0^{++}$. The pair must therefore be a $^3P_0$ state and an SU(3) singlet. Each final hadron contains one member of the pair. This model has the unique advantage of making definite predictions for all hadron vertices since all possible meson emissions are treated in a unified manner. The model contains a single arbitrary factor, the pair-creation constant γ, which must be determined from experiment. The QPCM predicts both $\pi N \rightarrow \pi\Delta$ and $\pi N \rightarrow \rho N$ amplitudes to be dominated by "anti-SU(6)$_W$" phases.

Most models of baryon decay share the weakness of being unable to predict either the masses or the SU(6)$\times$O(3) compositions of the decaying baryon resonances. Thus, the possibility of configuration mixing among various states causes some predictions of these models to be less

certain than others. Of course, mixing angles can be introduced as parameters to be determined experimentally, but this procedure is theoretically unsatisfactory. One model which has been very successful at solving the problems of baryon spectroscopy is the Isgur-Karl quark model.[6] This nonrelativistic quark model provides very good descriptions of baryons in the ground state as well as in the first and second excited states. In this model, baryons are described as bound states of three "constituent" quarks subjected to color hyperfine interactions suggested by quantum chromodynamics. The confining potential is assumed to be a flavor-independent function of the relative quark separation and is approximated by a harmonic-oscillator potential perturbed by an arbitrary anharmonic term. SU(3)$_{\text{flavor}}$ is broken by giving the strange quark a heavier mass than the up and down quarks, which are assumed to have the same mass. As with all models discussed here, the Isgur-Karl model can be criticized for its nonrelativistic treatment of quarks and hadrons.

The baryon compositions (mixing angles) predicted by the Isgur-Karl model have been used by Koniuk and Isgur[7] to calculate baryon decays by photon and pseudo-scalar meson emission. Rather than consider a specific dynamical model for the decay mechanism, they considered the case of elementary meson emission described by an effective interaction for $q \rightarrow qM$. Their meson-emission amplitudes contain an SU(6)$_W$-invariant part with coefficient g and a "recoil" term with coefficient h. It is of interest to note that, in the limit of elementary pseudoscalar meson emission, the QPCM leads to an effective interaction for pion emission similar to that used by Koniuk and Isgur if one takes $g \simeq -h$. This result is in good agreement with the fitted parameters Koniuk and Isgur obtained for describing the ground-state and negative-parity baryons. Thus, the $\pi\Delta$ couplings obtained from the QPCM are expected to agree with those of Koniuk and Isgur after allowing for configuration mixing.

Koniuk recently extended his earlier work with Isgur to include baryon decays by vector meson emission.[8] His effective interaction for elementary vector meson emission contains a spin-independent term with coefficient g' and a spin-dependent term with coefficient h' (primes added here to distinguish between pseudoscalar coefficients g and h). The QPCM leads to an effective interaction for elementary vector meson emission somewhat like Koniuk's if one takes $g' = \frac{1}{2}h'$ and includes a spin-dependent quark recoil term absent in his interaction. Koniuk finds $g' \simeq 0.4h'$, so that the QPCM prediction is again well satisfied.

F. Signs of resonant amplitudes:
Experiment versus theory

In Table VIII, we compare the experimental signs of resonant $\pi N \rightarrow \pi\Delta$ amplitudes determined from the Berkeley-SLAC,[1] Saclay,[2] Imperial College,[3] and present analyses. In Table IX, we compare the experimental signs of resonant $\pi N \rightarrow \rho N$ amplitudes and in Table X, we compare the experimental signs of resonant $\pi N \rightarrow \epsilon N$ amplitudes. Signs of the Berkeley-SLAC and Saclay amplitudes were obtained from coupled K-matrix analyses of

TABLE VIII. Experimental signs of resonant $\pi N \to \pi\Delta$ amplitudes determined from the Berkeley-SLAC (BS) (Ref. 1), Saclay (Ref. 2), Imperial College (IC) (Ref. 3), and present (VPI&SU) analyses. States are denoted by (mass) (D, L^P) (SU(3),SU(2)). An asterisk ($*$) marks those amplitudes which have unambiguous signs.

Amplitude	Classification	BS	Saclay	IC	VPI&SU
$SD\,11(\pi\Delta)$	(1535) $(70,1^-)$, (8,2)	+ (?)	0		0
$*SD\,11(\pi\Delta)$	(1650) $(70,1^-)$ (8,4)	+	+		+
$*DS\,13(\pi\Delta)$	(1520) $(70,1^-)$ (8,2)	−	−		−
$*DD\,13(\pi\Delta)$	(1520) $(70,1^-)$ (8,2)	−	−		−
$DS\,13(\pi\Delta)$	(1700) $(70,1^-)$ (8,4)	−	0		−(?)
$DD\,13(\pi\Delta)$	(1700) $(70,1^-)$ (8,4)	+	−(?)		+
$*DD\,15(\pi\Delta)$	(1675) $(70,1^-)$ (8,4)	+	+		+
$DG\,15(\pi\Delta)$	(1675) $(70,1^-)$ (8,4)				0
$*SD\,31(\pi\Delta)$	(1620) $(70,1^-)$ (10,2)	−	−	−	−
$*DS\,33(\pi\Delta)$	(1700) $(70,1^-)$ (10,2)	+	+	+	+
$*DD\,33(\pi\Delta)$	(1700) $(70,1^-)$ (10,2)	+ (?)	+	?	+
$*PP\,11(\pi\Delta)$	(1440) $(56,0^+)$ (8,2)	+	+		+
$*PP\,33(\pi\Delta)$	(1600) $(56,0^+)$ (10,4)	+	+	+	+
$PF\,33(\pi\Delta)$	(1600) $(56,0^+)$ (10,4)	0	−(?)	?	0
$PP\,11(\pi\Delta)$	(1710) $(70,0^+)$ (8,2)	+	−		−
$PP\,13(\pi\Delta)$	(1720) $(56,2^+)$ (8,2)	0	−		0
$PF\,13(\pi\Delta)$	(1720) $(56,2^+)$ (8,2)	0	0		0
$*FP\,15(\pi\Delta)$	(1680) $(56,2^+)$ (8,2)	−	−		−
$*FF\,15(\pi\Delta)$	(1680) $(56,2^+)$ (8,2)	+	+		+
$FP\,35(\pi\Delta)$	(1905) $(56,2^+)$ (10,4)	0			+
$*FF\,35(\pi\Delta)$	(1905) $(56,2^+)$ (10,4)	+			+
$*FF\,37(\pi\Delta)$	(1950) $(56,2^+)$ (10,4)	+			+

$\pi N \to \pi N$ and $\pi N \to \pi\pi N$.[34,38] For the Imperial College and present analyses, signs were obtained visually. In some cases, however, coupling signs for the present analysis were extracted by the fitting procedure used to generate the curves displayed in Figs. 4 and 6. All signs have been adjusted to comply with the baryon-first phase convention. The arbitrary overall sign for the four different analyses has been fixed by the $S_{31}(1620)$ coupling to the $\pi\Delta$ channel. When the size of the coupling is negligibly small, we give the sign as "0". When there are indications of large background in the vicinity of a resonance (i.e., when an amplitude at resonance is rotated more than 70° away from the imaginary axis), the sign is followed by a question mark in parentheses. In cases where the coupling may not be negligible but the sign is totally unknown, only a question mark is presented.

For the 22 $\pi\Delta$ couplings listed in Table VIII, the analyses agree for only 13 signs. Our criterion for agreement is for two or more analyses to find the same sign and no other analysis to conflict with that sign. If we consider the ρN couplings, the analyses strictly agree for only 5 signs out of the 36 listed. This poor agreement results from the smallness of most ρN couplings. We note that the analyses find 13 of the ρN couplings to be negligible. A good model for baryon decays should be able to explain the smallness of these couplings as well as the signs of larger resonant amplitudes. For the ϵN couplings, the analyses strictly agree for only two signs out of nine. In some cases, we can relax our criterion for strict agreement among the analyses. For example, we feel that the present and Saclay analyses reliably determine the signs of

$FF\,15(\rho_3 N)$ and $SD\,31(\rho_3 N)$, even though the Berkeley-SLAC analysis found these amplitudes to be negligible.

Tables VIII, IX, and X do not compare signs of $\pi N \to \pi N^*(P_{11})$ amplitudes since only one sign was available for comparison. For the $P_{33}(1600)$ resonance, both the Imperial College and present analyses found the sign of $PP\,33(\pi N^*)$ to be positive. The present work also found πN^* couplings to $S_{11}(1650)$, $S_{31}(1900)$, $P_{31}(1910)$, and $P_{33}(1920)$ with all signs positive. Our results for the πN^* channels can be compared with the SU(6)$_W$ prediction that the relative signs of all resonance couplings to the πN and $\pi N^*(P_{11})$ channels be the same. This prediction follows from the identical Clebsch-Gordan structure of decays into the radially excited state $(56,0^+)_2$ and the ground state $(56,0^+)_0$.

In Table XI, we present signs of resonant $\pi N \to \pi\Delta$ amplitudes predicted by the decay model of Koniuk and Isgur,[7] l-broken SU(6)$_W$ [both SU(6)$_W$-like and anti-SU(6)$_W$ signs],[4] and the QPCM.[5] In Table XII, we present signs of resonant $\pi N \to \rho N$ amplitudes predicted by the decay model of Koniuk,[8] l-broken SU(6)$_W$,[4] and the QPCM.[5] In Table XIII, we present signs of $\pi N \to \epsilon N$ amplitudes predicted by the QPCM. All theoretical signs have been adjusted to conform with the baryon-first phase convention. The arbitrary overall signs for the predictions have been fixed by the $D_{15}(1675)$ coupling to the $\pi\Delta$ channel and the $S_{31}(1620)$ coupling to $\rho_1 N$. In the absence of configuration mixing, decays must satisfy the SU(6) selection rule $l_f = L \pm 1$. Thus, when a coupling is predicted to be either forbidden or very small ($|A| < 0.01$), we give the sign as 0. Predictions of

TABLE IX. Experimental signs of resonant $\pi N \rightarrow \rho N$ amplitudes determined from the Berkeley-SLAC (BS) (Ref. 1), Saclay (Ref. 2), Imperial College (IC) (Ref. 3), and present (VPI&SU) analyses. States are denoted by (mass) (D,L^P) (SU(3),SU(2)). An asterisk ($*$) marks those amplitudes which have unambiguous signs.

Amplitude	Classification	BS	Saclay	IC	VPI&SU
$*SS\,11(\rho_1 N)$	(1535) $(70,1^-)$ (8,2)	−	−(?)		−
$SD\,11(\rho_3 N)$	(1535) $(70,1^-)$ (8,2)	0	0		0
$SS\,11(\rho_1 N)$	(1650) $(70,1^-)$ (8,4)	−(?)	+(?)		−
$SD\,11(\rho_3 N)$	(1650) $(70,1^-)$ (8,4)	0	+		+(?)
$DD\,13(\rho_1 N)$	(1520) $(70,1^-)$ (8,2)	0	0		0
$*DS\,13(\rho_3 N)$	(1520) $(70,1^-)$ (8,2)	−	−(?)		−
$DD\,13(\rho_3 N)$	(1520) $(70,1^-)$ (8,2)	0	0		0
$DD\,13(\rho_1 N)$	(1700) $(70,1^-)$ (8,4)	0	0		0
$DS\,13(\rho_3 N)$	(1700) $(70,1^-)$ (8,4)	+	−(?)		0
$DD\,13(\rho_3 N)$	(1700) $(70,1^-)$ (8,4)	0	0		0
$DD\,15(\rho_1 N)$	(1675) $(70,1^-)$ (8,4)	0	0		0
$DD\,15(\rho_3 N)$	(1675) $(70,1^-)$ (8,4)	0	−		−
$DG\,15(\rho_3 N)$	(1675) $(70,1^-)$ (8,4)				0
$*SS\,31(\rho_1 N)$	(1620) $(70,1^-)$ (10,2)	+	+	+	+
$SD\,31(\rho_3 N)$	(1620) $(70,1^-)$ (10,2)	0	−	?	−
$DD\,33(\rho_1 N)$	(1700) $(70,1^-)$ (10,2)	0	0	+	0
$DS\,33(\rho_3 N)$	(1700) $(70,1^-)$ (10,2)	−	+(?)	?	+
$DD\,33(\rho_3 N)$	(1700) $(70,1^-)$ (10,2)	0	0	?	0
$PP\,11(\rho_1 N)$	(1440) $(56,0^+)$ (8,2)	+	−(?)		0
$PP\,11(\rho_3 N)$	(1440) $(56,0^+)$ (8,2)	0	+		0
$PP\,33(\rho_1 N)$	(1600) $(56,0^+)$ (10,4)	0	+	?	0
$PP\,33(\rho_3 N)$	(1600) $(56,0^+)$ (10,4)	0	+	?	0
$PF\,33(\rho_3 N)$	(1600) $(56,0^+)$ (10,4)	0	0	?	0
$PP\,11(\rho_1 N)$	(1710) $(70,0^+)$ (8,2)	−	+		+
$PP\,11(\rho_3 N)$	(1710) $(70,0^+)$ (8,2)	0	+		0
$PP\,13(\rho_1 N)$	(1720) $(56,2^+)$ (8,2)	+	−		0
$PP\,13(\rho_3 N)$	(1720) $(56,2^+)$ (8,2)	0	+		0
$PF\,13(\rho_3 N)$	(1720) $(56,2^+)$ (8,2)	0	0		0
$FF\,15(\rho_1 N)$	(1680) $(56,2^+)$ (8,2)	0	0		0
$*FP\,15(\rho_3 N)$	(1680) $(56,2^+)$ (8,2)	−	−		−
$FF\,15(\rho_1 N)$	(1680) $(56,2^+)$ (8,2)	0	−		−
$FF\,35(\rho_1 N)$	(1905) $(56,2^+)$ (10,4)	0			0
$*FP\,35(\rho_3 N)$	(1905) $(56,2^+)$ (10,4)	+			+
$FF\,35(\rho_3 N)$	(1905) $(56,2^+)$ (10,4)	0			0
$FF\,37(\rho_1 N)$	(1950) $(56,2^+)$ (10,4)	0			0
$FF\,37(\rho_3 N)$	(1950) $(56,2^+)$ (10,4)	+(?)			0

TABLE X. Experimental signs of resonant $\pi N \rightarrow \epsilon N$ amplitudes determined from the Berkeley-SLAC (BS) (Ref. 1), Saclay (Ref. 2), and present (VPI&SU) analyses. States are denoted by (mass) (D,L^P) (SU(3),SU(2)). An asterisk ($*$) marks those amplitudes which have unambiguous signs.

Amplitude	Classification	BS	Saclay	VPI&SU
$*SP\,11(\epsilon N)$	(1535) $(70,1^-)$ (8,2)	+	+	+
$SP\,11(\epsilon N)$	(1650) $(70,1^-)$ (8,4)	+	0	+
$DP\,13(\epsilon N)$	(1520) $(70,1^-)$ (8,2)	−	−(?)	0
$DP\,13(\epsilon N)$	(1650) $(70,1^-)$ (8,4)	+	0	+
$DF\,15(\epsilon N)$	(1675) $(70,1^-)$ (8,4)	0	+	0
$PS\,11(\epsilon N)$	(1440) $(56,0^+)$ (8,2)	−(?)	−	+
$PS\,11(\epsilon N)$	(1710) $(70,0^+)$ (8,2)	−(?)	−	−(?)
$PD\,13(\epsilon N)$	(1720) $(56,2^+)$ (8,2)	0	−	0
$*FD\,15(\epsilon N)$	(1680) $(56,2^+)$ (8,2)	+	+	+

TABLE XI. Signs of resonant $\pi N \to \pi\Delta$ amplitudes predicted by the decay model of Koniuk and Isgur (Ref. 7), the QPCM (Ref. 5), and l-broken SU(6)$_W$ (Ref. 4). States are denoted by (mass) (D,L^P) (SU(3),SU(2)).

Amplitude	Classification			Koniuk-Isgur	QPCM	Anti-SU(6)$_W$	SU(6)$_W$
$SD\,11(\pi\Delta)$	(1535)	(70,1$^-$)	(8,2)	+	+	+	−
$SD\,11(\pi\Delta)$	(1650)	(70,1$^-$)	(8,4)	+	+	+	−
$DS\,13(\pi\Delta)$	(1520)	(70,1$^-$)	(8,2)	−	−	−	+
$DD\,13(\pi\Delta)$	(1520)	(70,1$^-$)	(8,2)	−	−	−	−
$DS\,13(\pi\Delta)$	(1700)	(70,1$^-$)	(8,4)	−	−	−	+
$DD\,13(\pi\Delta)$	(1700)	(70,1$^-$)	(8,4)	+	+	+	+
$DD\,15(\pi\Delta)$	(1675)	(70,1$^-$)	(8,4)	+	+	+	+
$DG\,15(\pi\Delta)$	(1675)	(70,1$^-$)	(8,4)	0	0	0	0
$SD\,31(\pi\Delta)$	(1620)	(70,1$^-$)	(10,2)	−	−	−	+
$DS\,33(\pi\Delta)$	(1700)	(70,1$^-$)	(10,2)	+	+	+	−
$DD\,33(\pi\Delta)$	(1700)	(70,1$^-$)	(10,2)	+	+	+	+
$PP\,11(\pi\Delta)$	(1440)	(56,0$^+$)	(8,2)	+	?	+	+
$PP\,33(\pi\Delta)$	(1600)	(56,0$^+$)	(10,4)	+	+	+	+
$PF\,33(\pi\Delta)$	(1600)	(56,0$^+$)	(10,4)	+ 0	0	0	0
$PP\,11(\pi\Delta)$	(1710)	(70,0$^+$)	(8,2)	−	?	−	−
$PP\,13(\pi\Delta)$	(1720)	(56,2$^+$)	(8,2)	−	−	−	−
$PF\,13(\pi\Delta)$	(1720)	(56,2$^+$)	(8,2)	+	−	−	+
$FP\,15(\pi\Delta)$	(1680)	(56,2$^+$)	(8,2)	−	+	+	−
$FF\,15(\pi\Delta)$	(1680)	(56,2$^+$)	(8,2)	+	+	+	+
$FP\,35(\pi\Delta)$	(1905)	(56,2$^+$)	(10,4)	+	−	−	+
$FF\,35(\pi\Delta)$	(1905)	(56,2$^+$)	(10,4)	+	+	+	+
$FF\,37(\pi\Delta)$	(1950)	(56,2$^+$)	(10,4)	+	+	+	+

SU(6)$_W$ and the QPCM assume unmixed SU(6)$\times$O(3) assignments for the resonances; however, predictions of Koniuk and Isgur[7,8] take mixing effects into account.

We first compare experimental and theoretical signs for $\pi N \to \pi\Delta$ amplitudes. The signs of the 13 $\pi N \to \pi\Delta$ amplitudes determined unambiguously from two or more analyses are correctly predicted only by the decay model of Koniuk and Isgur.[7] The predictions of anti-SU(6)$_W$ and the QPCM are wrong, however, only for $FP\,15(\pi\Delta)$. Their failure to correctly predict the sign of this amplitude can be explained by interpreting the observed $F_{15}(1680)$ resonance as a strong mixture of the states $(56,2^+)_2$ (8,2) and $(70,2^+)_2$ (8,2). Unbroken SU(6)$_W$ incorrectly predicts four signs including the sign of $DS\,33(\pi\Delta)$, which cannot be altered by mixing.

A new result of the present analysis is the sign of $FP\,35(\pi\Delta)$, which we find to be positive. This result agrees with the prediction of Koniuk and Isgur and disagrees with anti-SU(6)$_W$ and the QPCM. Since the Isgur-Karl model predicts the observed F_{35} resonance to be a strong mixture of the states $(56,2^+)_2$ (10,4) and $(70,2^+)_2$ (10,2), we can again attribute the failures of the QPCM and anti-SU(6)$_W$ to their neglect of mixing effects.

We next compare experimental and theoretical signs of resonant $\pi N \to \rho N$ amplitudes. The experimental analyses unambiguously determine the signs of seven amplitudes: $SS\,11(\rho_1 N)$, $SS\,31(\rho_1 N)$, $DS\,13(\rho_3 N)$, $FP\,15(\rho_3 N)$, $FF\,15(\rho_3 N)$, $SD\,31(\rho_3 N)$, and $FP\,35(\rho_3 N)$. Koniuk's model[8] correctly predicts all signs correctly except that of $FP\,35(\rho_3 N)$. This apparent failure combined with the pre-

dictions of Koniuk and Isgur[7,8] has a very interesting explanation. As discussed earlier, the Isgur-Karl model predicts two F_{35} resonances in this energy range, a mostly $(56,2^+)$ state at 1940 MeV and a mostly $(70,2^+)$ state at 1975 MeV. The $(56,2^+)$ state is predicted to have large πN and $\pi\Delta$ couplings with the signs observed experimentally. Its ρN couplings are predicted to be weak. In contrast, the $(70,2^+)$ state is predicted to have weak πN and $\pi\Delta$ couplings but a very strong ρN coupling and the predicted sign of $FP\,35(\rho_3 N)$ for the $(70,2^+)$ state agrees with experiment. We may conclude that the observed ρN decay is associated not with the $(56,2^+)$ resonance that dominates elastic scattering but with the $(70,2^+)$ resonance which, before now, had been thought to be unobserved.

As Tables XI and XII indicate, the QPCM predicts anti-SU(6)$_W$ signs to dominate both $\pi N \to \rho N$ and $\pi N \to \pi\Delta$ amplitudes. For the seven $\pi N \to \rho N$ amplitudes considered here, the QPCM predicts only $SD\,31(\rho_3 N)$ to have an SU(6)$_W$-like sign. We suggest that this sign may have been calculated incorrectly in Ref. 5. For $SS\,31(\rho_1 N)$, $SD\,31(\rho_3 N)$, and $DS\,13(\rho_3 N)$, the Isgur-Karl model predicts mixing effects to be small. As expected, Koniuk's predictions for these amplitudes have anti-SU(6)$_W$ signs, in agreement with the QPCM predictions. The remaining four amplitudes are subject to mixing effects so that the predictions of the QPCM and l-broken SU(6)$_W$ are less reliable.

Finally, we compare the theoretical and experimental predictions for resonant $\pi N \to \epsilon N$ amplitudes. Only the QPCM has addressed itself to these decays. In the ab-

TABLE XII. Signs of resonant $\pi N \to \rho N$ amplitudes predicted by the decay model of Koniuk (Ref. 8), by the QPCM (Ref. 5), and by l-broken SU(6)$_W$ (Ref. 4). States are denoted by (mass) (D,L^P) (SU(3),SU(2)).

Amplitude	Classification			Koniuk	QPCM	Anti-SU(6)$_W$	SU(6)$_W$
$SS\,11(\rho_1 N)$	(1535)	(70,1$^-$)	(8,2)	−	+	+	+
$SD\,11(\rho_3 N)$	(1535)	(70,1$^-$)	(8,2)	+	+	+	−
$SS\,11(\rho_1 N)$	(1650)	(70,1$^-$)	(8,4)	−	−	−	−
$SD\,11(\rho_3 N)$	(1650)	(70,1$^-$)	(8,4)	+	−	−	+
$DD\,13(\rho_1 N)$	(1520)	(70,1$^-$)	(8,2)	+	+	+	+
$DS\,13(\rho_3 N)$	(1520)	(70,1$^-$)	(8,2)	−	−	−	+
$DD\,13(\rho_3 N)$	(1520)	(70,1$^-$)	(8,2)	−	−	−	−
$DD\,13(\rho_1 N)$	(1700)	(70,1$^-$)	(8,4)	−0	−	−	−
$DS\,13(\rho_3 N)$	(1700)	(70,1$^-$)	(8,4)	−	+	+	−
$DD\,13(\rho_3 N)$	(1700)	(70,1$^-$)	(8,4)	−	+	−	−
$DD\,15(\rho_1 N)$	(1675)	(70,1$^-$)	(8,4)	−	−	−	−
$DD\,15(\rho_3 N)$	(1675)	(70,1$^-$)	(8,4)	−	−	−	−
$DG\,15(\rho_3 N)$	(1675)	(70,1$^-$)	(8,4)	0	0	0	0
$SS\,31(\rho_1 N)$	(1620)	(70,1$^-$)	(10,2)	+	+	+	+
$SD\,31(\rho_3 N)$	(1620)	(70,1$^-$)	(10,2)	−	+	−	+
$DD\,33(\rho_1 N)$	(1700)	(70,1$^-$)	(10,2)	+	+	+	+
$DS\,33(\rho_3 N)$	(1700)	(70,1$^-$)	(10,2)	+	+	+	−
$DD\,33(\rho_3 N)$	(1700)	(70,1$^-$)	(10,2)	+	?	+	+
$PP\,11(\rho_1 N)$	(1440)	(56,0$^+$)	(8,2)	+0	+	+	+
$PP\,11(\rho_3 N)$	(1440)	(56,0$^+$)	(8,2)	+0	?	−	−
$PP\,33(\rho_1 N)$	(1600)	(56,0$^+$)	(10,4)	−	?	−	−
$PP\,33(\rho_3 N)$	(1600)	(56,0$^+$)	(10,4)	−	?	−	−
$PF\,33(\rho_3 N)$	(1600)	(56,0$^+$)	(10,4)	−0	0	0	0
$PP\,11(\rho_1 N)$	(1710)	(70,0$^+$)	(8,2)	+	+	+	+
$PP\,11(\rho_3 N)$	(1710)	(70,0$^+$)	(8,2)	+	?	−	−
$PP\,13(\rho_1 N)$	(1720)	(56,2$^+$)	(8,2)	+	+	+	+
$PP\,13(\rho_3 N)$	(1720)	(56,2$^+$)	(8,2)	−	+	+	+
$PF\,13(\rho_3 N)$	(1720)	(56,2$^+$)	(8,2)	−	+	+	−
$FF\,15(\rho_1 N)$	(1680)	(56,2$^+$)	(8,2)	+	+	+	+
$FP\,15(\rho_3 N)$	(1680)	(56,2$^+$)	(8,2)	−	−	−	+
$FF\,15(\rho_3 N)$	(1680)	(56,2$^+$)	(8,2)	−	−	−	−
$FF\,35(\rho_1 N)$	(1905)	(56,2$^+$)	(10,4)	−0	−	−	−
$FP\,35(\rho_3 N)$	(1905)	(56,2$^+$)	(10,4)	−	+	+	−
$FF\,35(\rho_3 N)$	(1905)	(56,2$^+$)	(10,4)	−	−	−	−
$FF\,37(\rho_1 N)$	(1950)	(56,2$^+$)	(10,4)	−	−	−	−
$FF\,37(\rho_3 N)$	(1950)	(56,2$^+$)	(10,4)	−	−	−	−

sence of configuration mixing, the QPCM predicts the $D_{15}(1675)$ resonance to decouple from $DF15(\epsilon N)$ and the $P_{11}(1710)$ resonance to decouple from $PS11(\epsilon N)$. Experimentally, $DF15(\epsilon N)$ is found to be negligibly small in the

TABLE XIII. Signs of resonant $\pi N \to \epsilon N$ amplitudes predicted by the QPCM (Ref. 5). States are denoted by (mass) (D,L^P) (SU(3),SU(2)).

Amplitude	Classification			QPCM
$SP\,11(\epsilon N)$	(1535)	(70,1$^-$)	(8,2)	−
$SP\,11(\epsilon N)$	(1650)	(70,1$^-$)	(8,4)	−
$DP\,13(\epsilon N)$	(1520)	(70,1$^-$)	(8,2)	−
$DP\,13(\epsilon N)$	(1650)	(70,1$^-$)	(8,4)	−
$DF\,15(\epsilon N)$	(1675)	(70,1$^-$)	(8,4)	0
$PS\,11(\epsilon N)$	(1440)	(56,0$^+$)	(8,2)	?
$PS\,11(\epsilon N)$	(1710)	(70,0$^+$)	(8,2)	0
$PD\,13(\epsilon N)$	(1720)	(56,2$^+$)	(8,2)	−
$FD\,15(\epsilon N)$	(1680)	(56,2$^+$)	(8,2)	−

Berkeley-SLAC, Saclay, and present analyses. The experimental situation is unclear, however, for the $P_{11}(1710)$ coupling to $PS11(\epsilon N)$. The present analysis finds this coupling small whereas the Berkeley-SLAC and Saclay analyses find it large. The experimental analyses unambiguously determine the signs of only two $\pi N \to \epsilon N$ amplitudes, $SP11(\epsilon N)$ and $FD15(\epsilon N)$. Both signs are incorrectly predicted by the QPCM. Unfortunately, strong mixing for the S_{11} and F_{15} states causes these predictions to be somewhat unreliable. We tentatively conclude that the QPCM fails to correctly describe the ϵN decay mode of baryons. Recent quark-model calculations by Jaffe[39] and others[40] suggest a possible explanation for this apparent failure. If the ϵ meson is an $L=0$ $u\bar{u}d\bar{d}$ configuration rather than an $L=1$ $q\bar{q}$ state, then the QPCM is not applicable for hadron decays into ϵN. Indeed, a P-matrix analysis[41] of elastic $\pi\pi$ scattering finds a pole in the $I_{\pi\pi}=0$ amplitude at 690 MeV. This pole can be identified with the ϵ meson which plays an important role in

low-energy $\pi N \rightarrow \pi \pi N$ reactions. The same P-matrix analysis also found a pole at 1040 MeV in the $I_{\pi\pi}=2$ amplitude. This pole can be associated with an exotic meson which we call ϵ_2. Both ϵ and ϵ_2 are expected to be broad resonances because of their "fall-apart" decays into two pions. The failure of our fits to correctly reproduce the experimental $\pi^+p \rightarrow \pi^+\pi^+n$ cross section above 1700 MeV (after considering several πN^* decay modes) might be due to our neglect of the exotic $\epsilon_2 N$ decay channel. Of course, there could be other explanations for this failure such as the need for a significant OPE contribution in the $I_{\pi\pi}=2$ channel. Work by Novoseller[27] and the Imperial College group[3] suggests, however, that such a contribution is probably small.

VIII. CONCLUSIONS

We have performed an energy-independent, isobar-model, partial-wave analysis of $\pi^-p \rightarrow \pi^+\pi^-n$, $\pi^-p \rightarrow \pi^0\pi^-p$, $\pi^+p \rightarrow \pi^0\pi^+p$, and $\pi^+p \rightarrow \pi^+\pi^+n$ at 22 energies between 1320 and 1930 MeV. The analysis includes over 30% more events than the previous Berkeley-SLAC analysis. We believe the present analysis to be the most extensive of its kind because of its wide energy range, high statistics, inclusion of the $\pi^+\pi^+n$ channel, consideration of πN^* decay channels, and search for g-wave amplitudes. Our work is independent of any elastic analyses since our amplitudes were not constrained by their results. Our solution corroborates many features seen in previous analyses by the Berkeley-SLAC, Saclay, and Imperial College groups and helps to resolve some of their differences. In particular, the present analysis agrees with the Saclay analysis regarding the importance of $FF15(\rho_3N)$ and $SD31(\rho_3N)$. For six coupling signs for which the Berkeley-SLAC and Saclay analyses found different results, the present work agrees with that of the Saclay group for the coupling signs of $P_{11}(1710)$ to $PP11(\rho_1N)$ and $PP11(\pi\Delta)$, for $D_{13}(1520)$ to $DP13(\epsilon N)$, for $D_{13}(1700)$ to $DS13(\rho_3N)$, and for $D_{33}(1700)$ to $DS33(\rho_3N)$. The present work agrees with the Berkeley-SLAC analysis, however, for the coupling sign of $S_{11}(1650)$ to $SS11(\rho_1N)$. Unlike in the Berkeley-SLAC solution, our $FF37(\pi\Delta)$ amplitude does not require a large background but our $FP35(\rho_3N)$ wave differs in phase from the elastic F_{35} wave. This difference may be ascribed to the existence of a highly inelastic second F_{35} resonance which decays dominantly to the ρN channel and only weakly to the πN channel. The Berkeley-SLAC collaboration used $FP35(\rho_3N)$ to help determine their overall phase above 1730 MeV. Their determination of the overall phase may therefore have been incorrect in that energy range if indeed there are two F_{35} resonances as discussed above. Finally, we note that the present results agree with the low-energy work of Arndt et al.[12]

The $\pi N^*(P_{11})$ channel was found to become important above about 1600 MeV and to be associated with inelasticity in the S_{11}, S_{31}, P_{31}, and P_{33} partial waves. To reliably determine couplings to this and other πN^* channels, new data are needed, especially for the $\pi^+\pi^+n$ channel which couples strongly to πN^* channels. It would be desirable to have new experiments to measure several thousand events for this channel at several closely spaced energies between 1700 and 2000 MeV. There is also a need for precise measurements of the $\pi^+p \rightarrow \pi^+\pi^+n$ cross section in this energy range. Additional data between 1800 and 2000 MeV for other charge channels could help establish several resonances predicted to belong to the $(70,2^+)_2$ and $(56,1^-)_3$ multiplets.

From the experimentally well-determined signs of resonant $\pi N \rightarrow \pi\Delta$ and $\pi N \rightarrow \rho N$ amplitudes, we infer that low-mass nonstrange excited-state baryons decay dominantly by $\Delta L_z = \pm 1$ transitions. This result is consistent with predictions of the QPCM and the anti-SU(6)$_W$ alternative of l-broken SU(6)$_W$. Occasional failures of these models to predict the correct signs for $\pi N \rightarrow \pi\Delta$ and $\pi N \rightarrow \rho N$ amplitudes can be attributed to their neglect of configuration mixing. The decay models of Koniuk and Isgur have been shown to correctly predict the signs of all well-determined $\pi N \rightarrow \pi\Delta$ and $\pi N \rightarrow \rho N$ amplitudes by taking mixing effects into account via the Isgur-Karl model. The experimental situation regarding signs of $\pi N \rightarrow \epsilon N$ amplitudes is unsatisfactory since the major analyses agree only for the signs of $SP11(\epsilon N)$ and $FD15(\epsilon N)$. The signs of both amplitudes are predicted incorrectly by the QPCM. We tentatively attribute this failure to the dipion (four-quark) composition of the ϵ meson. However, there could be other explanations such as disregard of the QPCM predictions for effects of configuration mixing.

The present work suggests that possible unestablished resonances[42] exist near 1900 MeV in the S_{11}, P_{11}, P_{13}, and F_{15} partial waves. Recent elastic analyses corroborate some of these findings. For the purpose of interpreting the growing body of information about resonances in the 1800—2100-MeV mass region, we suggest that the Isgur-Karl model be used to calculate the mass spectrum of negative-parity baryons in the $N=3$ band and to predict couplings signs and partial widths for baryon decays involving pseudoscalar, vector, and scalar mesons. The predictions should be carried out for all baryons through the $N=3$ band. We recommend that such calculations use the effective interactions for elementary meson emission suggested by the QPCM.

With the completion of this work, the major experimental features of the $\pi N \rightarrow \pi\pi N$ reaction below 1700 MeV may be considered to be well understood. Our analysis suggests a richer resonance structure between 1700 and 2000 MeV than revealed by πN elastic analyses. The partial-wave amplitudes provided by this analysis should furnish critical tests of models of baryon spectroscopy and decays.

*Present address: 30071 Cartier Drive, Rancho Palos Verdes, CA 90274.

[1]D. J. Herndon et al., Phys. Rev. D 11, 3183 (1975).

[2]J. Dolbeau, F. A. Triantis, M. Neveu, and F. Cadiet, Nucl. Phys. B108, 365 (1976).

[3]K. W. J. Barnham et al., Nucl. Phys. B168, 243 (1980). See also K. W. J. Barnham, in Proceedings of the Topical Conference on Baryon Resonances, Oxford, 1976, edited by R. T. Ross and D. H. Saxon (Rutherford Laboratory, Chilton, Didcot, England, 1977), pp. 109–137.

[4]W. P. Peterson and J. L. Rosner, Phys. Rev. D 6, 820 (1972); 7, 747 (1973); D. Faiman and J. Rosner, Phys. Lett. 45B, 357 (1973); David Faiman, Nucl. Phys. B77, 443 (1974).

[5]A. Le Yaouanc, L. Oliver, O. Pène, and J.-C. Raynal, Phys. Rev. D 8, 2223 (1973); 9, 1415 (1974); 11, 1272 (1975). Early work on the QPC (quark-pair-creation) model is discussed by L. Micu, Nucl. Phys. B10, 521 (1969).

[6]Nathan Isgur and Gabriel Karl, Phys. Rev. D 18, 4187 (1978); 19, 2653 (1979); 20, 1191 (1979).

[7]Roman Koniuk and Nathan Isgur, Phys. Rev. D 21, 1868 (1980).

[8]Roman Koniuk, Nucl. Phys. B195, 452 (1982).

[9]U. Mehtani et al., Phys. Rev. Lett. 29, 1634 (1972). See also Y. Williamson et al., ibid. 29, 1353 (1972).

[10]S. L. Baker et al., Nucl. Phys. B41, 91 (1972); J. Dolbeau, M. Neveu, F. A. Triantis, and C. Coutures, ibid. B78, 233 (1974); P. L. Jain, Z. Ahmad, and G. Pappas, Phys. Rev. D 15, 3181 (1977).

[11]Peter C. A. Newcomb, Phys. Rev. 132, 1283 (1963); W. J. Metzger, B. Forman, A. C. Melissinos, and T. Yamanouchi, ibid. 164, 1680 (1967); J. Debaisieux et al., Nucl. Phys. B5, 147 (1968); M. De Beer et al., ibid. B12, 599 (1969); B12, 617 (1969); M. G. Bowler and R. J. Cashmore, ibid. B17, 331 (1970); A. D. Brody et al., Phys. Rev. D 4, 2693 (1971).

[12]R. A. Arndt et al., Phys. Rev. D 20, 651 (1979). See also R. Aaron et al., Phys. Rev. Lett. 44, 66 (1980).

[13]Y. Goradia, LBL Report No. 3628, 1975 (unpublished). See also Y. Goradia and T. A. Lasinski, Phys. Rev. D 15, 220 (1977); Ronald Aaron et al., ibid. 16, 50 (1977).

[14]R. Aaron and R. D. Amado, Phys. Rev. Lett. 31, 1157 (1973).

[15]Ronald Aaron et al., Phys. Rev. D 12, 1984 (1975).

[16]I. J. R. Aitchison and R. J. A. Golding, Phys. Lett. 59B, 288 (1975).

[17]I. J. R. Aitchison and J. J. Brehm, Phys. Rev. D 20, 1119 (1979); 20, 1131 (1979).

[18]J. M. Blatt and V. F. Weisskopf, Theoretical Nuclear Physics (Wiley, New York, 1952).

[19]F. von Hippel and C. Quigg, Phys. Rev. D 5, 624 (1972).

[20]R. S. Longacre, Phys. Rev. D 19, 404 (1979).

[21]Kenneth M. Watson, Phys. Rev. 88, 1163 (1952).

[22]Y. Goradia, Phys. Rev. D 15, 1368 (1977); Y. Goradia and R. A. Arndt, ibid. 19, 2057 (1979).

[23]William J. Willis, Phys. Rev. 116, 753 (1959); I. Derado and N. Schmitz, ibid. 118, 309 (1960); W. A. Perkins, III et al., ibid. 118, 1364 (1960); Yu. A. Batusov et al., Zh. Eksp. Teor.

Fiz. 40, 1528 (1961) [Sov. Phys. JETP 13, 1070 (1961)]; J. Brisson et al., in International Conference on Elementary Particles, Aix-en-Provence, 1961, edited by E. Cremieu-Alcon et al. (Centre d'Etudes Nucleaires de Saclay, Seine-et-Oise, France, 1961), Vol. 1, p. 45; J. Deahl et al., Phys. Rev. 124, 1987 (1961); D. Stonehill et al., Phys. Rev. Lett. 6, 624 (1961); Janos Kirz, Joseph Schwartz, and Robert D. Tripp, Phys. Rev. 126, 763 (1962); R. Barloutaud et al., Nuovo Cimento 26, 1409 (1962); 27, 238 (1963); J. Alitti et al., ibid. 29, 515 (1963); V. Barnes et al., CERN Report No. 63-27, 1963 (unpublished); T. D. Blokhintseva et al., Zh. Eksp. Teor. Fiz. 44, 498 (1963) [Sov. Phys. JETP 17, 340 (1963)]; Janos Kirz, Joseph Schwartz, and Robert D. Tripp, Phys. Rev. 130, 2481 (1963); E. Pickup et al., ibid. 132, 1819 (1963); B. C. Barish et al., ibid. 135, B416 (1964); T. Blokhintseva et al., in Proceedings of the Twelfth International Conference on High Energy Physics, Dubna, 1964, edited by Ya. A. Smorodinskii et al. (Atomizdat, Moscow, 1965); J. F. Detoeuf et al., Phys. Rev. 134, B228 (1964); C. N. Vittitoe et al., ibid. 135, B232 (1964); Yu. A. Batusov, S. Bunyatov, V. Sidorov, and V. Jarba, Yad. Fiz. 1, 526 (1965) [Sov. J. Nucl. Phys. 1, 374 (1965)]; R. A. Burnstein et al., Phys. Rev. 137, B1044 (1965); J. Debaisieux et al., Nucl. Phys. 63, 273 (1965); L. Bertanza, A. Bigi, R. Carrara, and R. Casali, Nuovo Cimento 44A, 712 (1966); N. M. Cason et al., Phys. Rev. 150, 1134 (1966); P. Daronian et al., Nuovo Cimento 41A, 503 (1966); J. F. Detoeuf et al., Phys. Rev. Lett. 16, 860 (1966); John D. Oliver, I. Nadelhaft, and G. B. Yodh, Phys. Rev. 147, 932 (1966); C. P. Poirier et al., ibid. 143, 1092 (1966); 148, 1311 (1966); C. A. Tilger et al., ibid. 142, 972 (1966); C. B. Chiu et al., ibid. 156, 1415 (1967); S. Feminò, S. Jannelli, and F. Mezzanares, Nuovo Cimento 52A, 892 (1967); P. Chavanon, M. Crozon, T. Leray, and J. Tocqueville, Phys. Lett. 28B, 296 (1968); R. T. Van de Walle et al., Nuovo Cimento 53A, 745 (1968); F. Bulos et al., Phys. Rev. 187, 1827 (1969); A. Skuja et al., Phys. Rev. Lett. 31, 653 (1973); J. A. Jones, W. W. M. Allison, and D. H. Saxon, Nucl. Phys. B83, 93 (1974); A. V. Kravtsov et al., Yad. Fiz. 20, 942 (1974) [Sov. J. Nucl. Phys. 20, 500 (1975)]; Yu. A. Batusov et al., Yad. Fiz. 21, 308 (1975) [Sov. J. Nucl. Phys. 21, 162 (1975)]; D. I. Sober et al., Phys. Rev. D 11, 1017 (1975); S. A. Bunyatov et al., Yad. Fiz. 25, 325 (1977) [Sov. J. Nucl. Phys. 25, 177 (1977)]; A. V. Kravtsov et al., Nucl. Phys. B134, 413 (1978); A. A. Bel'Kov et al., Yad. Fiz. 31, 181 (1980) [Sov. J. Nucl. Phys. 31, 96 (1980)]; C. W. Bjork et al., Phys. Rev. Lett. 44, 62 (1980).

[24]B. J. VerWest and R. A. Arndt, Phys. Rev. C 25, 1979 (1982).

[25]G. Höhler, F. Kaiser, R. Koch, and E. Pietarinen, Handbook of Pion-Nucleon Scattering (Fachinformationszentrum, Karlsruhe, 1979), Physik Daten No. 12-7.

[26]R. E. Cutkosky, C. P. Forsyth, R. E. Hendrick, and R. L. Kelly, Phys. Rev. D 20, 2839 (1979).

[27]Daniel E. Novoseller, Nucl. Phys. B137, 445 (1978).

[28]Particle Data Group, Phys. Lett. 111B, 1 (1982).

[29]Richard A. Arndt et al., Phys. Rev. D 28, 97 (1983).

[30]A. D. Brody et al., Phys. Lett. 34B, 665 (1971).

[31]A. H. Rosenfeld et al., Phys. Lett. 55B, 486 (1975).

[32]M. De Beer et al., Nucl. Phys. B12, 599 (1969); P. Chavanon, J. Dolbeau, and G. Smadja, ibid. B76, 157 (1974).

[33]D. Faiman, J. L. Rosner, and J. Weyers, Nucl. Phys. B57, 45 (1973); R. J. Cashmore, D. W. G. S. Leith, R. S. Longacre, and A. H. Rosenfeld, ibid. B92, 37 (1975).

[34]R. S. Longacre and J. Dolbeau, Nucl. Phys. B122, 493 (1977).

[35]H. J. Lipkin and S. Meshkov, Phys. Rev. Lett. 14, 670 (1965).

[36]F. J. Gilman, M. Kugler, and S. Meshkov, Phys. Lett. 45B, 481 (1973); Phys. Rev. D 9, 715 (1974).

[37]H. J. Melosh, Phys. Rev. D 9, 1095 (1974).

[38]R. S. Longacre et al., Phys. Lett. 55B, 415 (1975); Phys. Rev. D 17, 1795 (1978).

[39]R. L. Jaffe, Phys. Rev. D 15, 267 (1977).

[40]John Weinstein and Nathan Isgur, Phys. Rev. D 27, 588 (1983).

[41]R. L. Jaffe and F. E. Low, Phys. Rev. D 19, 2105 (1979).

[42]We refer to any baryon resonance as unestablished which the Particle Data Group (Ref. 28) has not given either three- or four-star status.